CHEMISTRY
A EUROPEAN JOURNAL

DOI: 10.1002/chem.200601193

Functional [6]Pericyclynes: Aromatization to Substituted *carbo*-Benzenes**

Catherine Saccavini, Christine Sui-Seng, Luc Maurette, Christine Lepetit, Sabine Soula, Chunhai Zou, Bruno Donnadieu, and Remi Chauvin*[a]

Abstract: Reductive treatment of stereoisomeric mixtures of variously substituted hexaoxy[6]pericyclynes with $SnCl_2$/HCl led to the corresponding substituted *carbo*-benzenes. Tetramethoxyhexaphenyl[6]pericylynediol and dimethoxyhexaphenyl[6]pericyclynetetrol thus proved to be alternative precursors of hexaphenyl-*carbo*-benzene, previously described. Another hexaaryl-*carbo*-benzenic chromophore with 4-pyridyl and 4-anisyl substituents was targeted for its second-order nonlinear optical properties and was obtained by aromatization of a dimethoxy[6]pericyclynetetrol. Two alkynyl substituents in *para* positions were also found to be compatible with the C_{18} *carbo*-benzene ring, provided that the four remaining vertices are substituted by phenyl groups. In the protected series, bis(trimethylsilylethynyl)hexaphenyl-*carbo*-benzene ($C_{18}Ph_4(C{\equiv}C{-}TMS)_2$) could be isolated and fully characterized, even by X-ray crystallography. In the bis-terminal series, the diethynylhexaphenyl-*carbo*-benzene $C_{18}Ph_4(C{\equiv}C{-}H)_2$ could not be isolated in the pure form. It could, however, be generated by two different methods and identified by the corresponding ^1H NMR spectra. Unsubstituted *carbo*-benzene $C_{18}H_6$ remains unknown, but tetraphenyl-*carbo*-benzenes $C_{18}Ph_4H_2$ with two unsubstituted vertices proved to be viable molecules. Whereas the "*para*" isomer could be characterized by MS and ^1H and ^{13}C NMR spectroscopy only in a mixture with polymeric materials, the "*ortho*" isomer (with adjacent CH vertices) could be isolated, and its structure was determined by using X-ray crystallography. The structure calculated at the B3PW91/6-31G** level of theory turned out to be in excellent agreement with the experimental structure. The ^1H and ^{13}C NMR chemical shifts of hexa- and tetraphenyl-*carbo*-benzenes were also calculated at the B3LYP/6-31+G** level of theory and were found to correlate with experimental spectra. The remote NMR deshielding of peripheral protons (through up to five bonds) revealed a very strong diatropic circulation around the C_{18} ring, regardless of the substitution pattern. In full agreement with theoretical investigations, it has been demonstrated experimentally that the *carbo*-benzene ring is "independently" aromatic, in accord with structural–energetic and –magnetic criteria.

Keywords: alkynes · aromaticity · aromatization · *carbo*-benzene · cumulenes · macrocycles

Introduction

The *carbo*-meric principle is a generalization and a unification of the ethynylogue and even cumulogue concepts.[1] It is rooted in Scott's early definition of pericyclynes, which are paradigms of ring *carbo*-mers of the ethynylogue type.[2] Ring *carbo*-mers of pure cumulogue type are degenerate (e.g., the cyclo[3*n*]carbon atoms), but hybrid ring *carbo*-mers of the ethynylogue–cumulogue type are encountered in the Kekulé forms of *carbo*-[*n*]annulenes which have been systematically studied at the density functional theory (DFT) level.[3,4] Beyond the indirect mass spectroscopic evidence of the case $n=5$ (*carbo*-cyclopentadienylium derivative),[5] the case $n=6$ (*carbo*-benzene derivatives) has only been experimentally attempted by one of us,[6] and definitively exemplified by Kuwatani, Ueda, and co-workers.[7] In the envisioned synthetic strategies,[5–7] the *carbo*-[*n*]annulenic structures ($n=5$, 6) were targeted by direct "aromatization" of [*n*]pericyclynic precursors. In particular, Kuwatani, Ueda, and co-workers showed that aryl-substituted *carbo*-

[a] Dr. C. Saccavini, Dr. C. Sui-Seng, Dr. L. Maurette, Dr. C. Lepetit, S. Soula, Dr. C. Zou, Dr. B. Donnadieu, Prof. R. Chauvin
Laboratoire de Chimie de Coordination du CNRS, UPR 8241
205 Route de Narbonne 31077, Toulouse cedex 4 (France)
Fax: (+33) 561-333-113
E-mail: chauvin@lcc-toulouse.fr

[**] Series title, Part 2; for Part 1, see: C. Saccavini, C. Tedeschi, L. Maurette, C. Sui-Seng, C. Zou, M. Soleilhavoup, L. Vendier, R. Chauvin, *Chem. Eur. J.* **2007**, *13*, DOI: 10.1002/chem.200601191.

Supporting information for this article is available on the WWW under http://www.chemeurj.org/ or from the author.

benzene hydrocarbons **1a**–**1d** can be obtained by reductive treatment of various hexaoxy[6]pericyclynes **2a–f** with $SnCl_2$/HCl (Scheme 1).[7] The latter reagent has long been used to generate butatrienes from substituted but-2-yne-1,4-diols[8] and the Kekulé forms of *carbo*-benzene indeed feature three butatriene edges alternating with three but-2-yne edges pre-existing in the hexaoxy[6]pericyclyne precursors (Scheme 1).

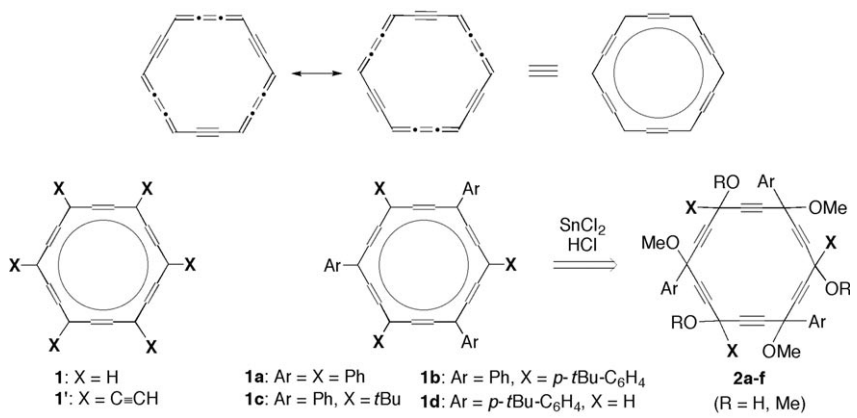

Scheme 1. Top: Delocalized representation of the superimposition of the Kekulé resonance forms of the *carbo*-benzene rings. Bottom left: Theoretical parent ring *carbo*-mer **1**[1,6] and total *carbo*-mer **1′**[1,9] of the benzene molecule.[4] Bottom right: experimental star-shaped *carbo*-benzene derivatives **1a**–**d** obtained by reductive aromatization of hexaoxy[6]pericyclyne precursors.[7]

Whereas unsubstituted *carbo*-benzene **1** ($C_{18}H_6$) remains a fictitious molecule (Scheme 1),[6] four aryl-substituted hydrocarbon derivatives **1a**–**d** with a star-shaped substitution pattern (of idealized D_{6h} or "*meta*" D_{3h} symmetry) have been reported.[7] In one of them (**1d**), three nonadjacent unsubstituted C–H vertices are present. The next challenge was therefore three-fold. 1) To synthesize *carbo*-benzene derivatives with other axial substitution patterns and in particular with idealized "*para*" C_{2v} or D_{2h} symmetry. 2) To extend the substituent compatibility of the *carbo*-benzene ring, first to heteroatom-containing aryl substituents. In order to get closer to the parent theoretical *carbo*-benzene **1**[3,4] or to the total *carbo*-mer of benzene **1′** (Scheme 1),[1,9] substitution patterns with adjacent unsubstituted C–H vertices or alkynyl substituents, respectively, are particularly attractive. 3) To compare experimental and theoretical results on strictly identical structures. The first goal was to directly validate the level of calculation employed in previous theoretical studies (B3PW91/6-31G**). The second goal was then to analyze the influence of substitution on the apparent macrocyclic "aromaticity" of *carbo*-benzene derivatives.

Results and Discussion

The eight novel hexaoxy[6]pericyclynes **3a**–**g** described in the preceding report were actually designed as precursor candidates for the generation of *carbo*-benzene derivatives **4a**–**e**,**g** (Scheme 2).[10] In order to facilitate reading of the two papers, the same compound numbering has been adopted in both reports. Note also that **4a** and **1a** are the same molecule, namely hexaphenyl-*carbo*-benzene.

Synthesis and characterization of the *carbo*-benzene derivatives: The hexaoxy[6]pericyclyne derivatives **3a–g** correspond to six different substitution patterns. Their intrinsic chemical value is limited by the fact that they were obtained as

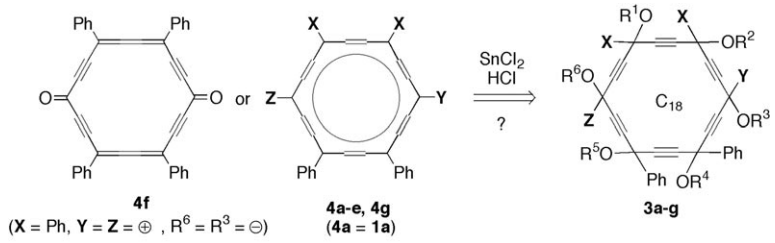

Scheme 2. *Carbo*-benzene derivatives with novel substitution patterns as targeted from previously described hexaoxy[6]pericyclynes (the compound numbering adopted herein is the same as that used in the preceding report).[10]

mixtures of stereoisomers.[10] The stereochemical disorder can however be cancelled by converting stereogenic sp^3 vertices to sp^2 vertices, either partly through oxidation of secondary carbinol vertices (as in the pericyclynedione **3f** from pericyclynediol **3e**),[10] or completely through reductive aromatization. The procedure of Kuwatani, Ueda, and co-workers for the generation of aryl-substituted *carbo*-benzenes of three-fold "*meta*" symmetry **1a–d** (Scheme 1)[7] from the [6]pericyclynes **3a–e**,**g** is envisioned here.

Hexaphenyl-carbo-*benzene **1a** from **3a** and **3a′***: The hexaphenyl-*carbo*-benzene **1a** has been described in detail by Kuwatani, Ueda, and co-workers,[7b] and it can be regarded as a reference compound in this series. These authors prepared this compound by reductive aromatization of the [6]pericyclynetriol **5c** possessing alternating C(Ph)OH and C(Ph)OMe vertices.[10] The applicability of the aromatization process has thus been attempted with [6]pericyclynetetrol **3a** and [6]pericyclynediol **3a′**, both possessing adja-

cent CPhOH vertices (Scheme 3). We found that treatment of **3a** or **3a′** with a large excess of $SnCl_2$ in ethereal HCl also afforded hexaphenyl-*carbo*-benzene **1a**, along with

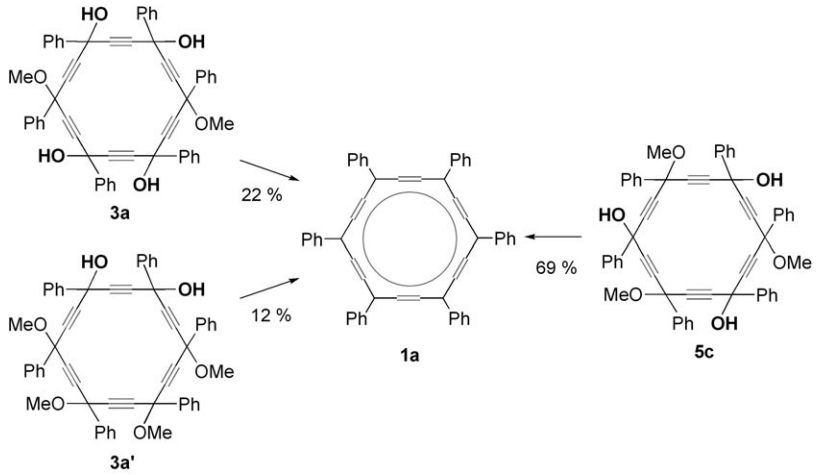

Scheme 3. Reductive aromatization of three different hexaphenylhexaoxy[6]pericyclynes to hexaphenyl-*carbo*-benzene **1a** with the $SnCl_2$/HCl reagent in diethyl ether at 0–20 °C. The conversion **5c**→**1a** is included for comparison.[7]

polymeric material. After chromatography with chloroform as eluent, the target compound was obtained in the less polar red-orange fractions and identified by comparison of its ^{1}H NMR spectrum with the previously reported spectrum of **1a**.[7b] The aromatization process yields reached a maximum of 22 % from tetrol **3a** and 12 % from diol **3a′**, whereas a yield of 69 % was obtained from triol **5c** (Scheme 3).[7b]

The alternation of C(Ph)OH and C(Ph)OMe vertices is thus seemingly an advantageous topographical feature, but the aromatization yield might also depend on the undetermined stereochemical composition. Considering the overall preparation yield, however, recourse to the tetrol intermediate **3a** through a [14+4] strategy (2 %)[10] does compete with Kuwatani, Ueda, and co-workers synthesis based on the triol **5c** through an [11+7] strategy (1.5 %).[7b] Moreover, the [14+4] route provides a definite improvement in terms of the number of steps: Nine (through **3a**) instead of 16 (through **5c**).

Recrystallization of **1a** from chloroform afforded single crystals, but several attempts at reproducing X-ray diffraction analysis (previously reported by Kuwatani, Ueda, and co-workers, but not listed in the Cambridge Crystal Data Centre)[7b] were unsuccessful owing to weak diffraction intensities. A more accurate insight into the frozen equilibrium structure of **1a** was thus targeted through DFT calculations at the B3PW91/6-31G** level of theory. The results are detailed later.

The ^{1}H NMR and UV/Vis spectra of **1a** provided evidence of strong magnetic aromaticity and overall electronic delocalization in the solution structure.[7b] This interpretation was further confirmed by excellent agreement between the experimental ^{1}H and ^{13}C NMR chemical shifts and the corresponding values calculated at the B3LYP/6-31+G** level of theory (see both the discussion and Table 5 and Figure 13 below).

Pyridylanisyltetraphenyl-carbo-*benzene **4b** from **3b***: Hexaaryl substitution is a priori a stabilizing factor of the D_{6h} *carbo*-benzene ring. Whereas apolar representatives **1a** and **1b** with idealized D_{6h} and D_{3h} symmetry are known,[7] dipolar representatives with idealized C_{2v} symmetry are not. The "*para*"-dipolar *carbo*-benzene derivatives with idealized C_{2v} symmetry, such as the ring *carbo*-mer of *p*-nitroaniline, were theoretically envisioned as second-order nonlinear optic (NLO) chromophores of high quadratic hyperpolarizability.[11] Since direct anchoring of nitrogen-centered NR_2/NO_2 donor/acceptor substituents on the C_{18} ring is a rather futuristic synthetic challenge, carbon-anchored aromatic donor/acceptor substituents resembling the phenyl substituents of **1a** and **1b** were envisioned.[12] The *p*-anisyl/4-pyridyl (4-MeO-C_6H_4/4-C_5H_4N) substituent pair is a versatile candidate since its moderate push–pull character could be a posteriori enhanced by formal *trans* quaternization to the zwitterionic phenolate/pyridinium pair 4-$^-$O-C_6H_4/4-$C_5H_4N^+$-Me (possibly mediated by treatment with BBr_3/MeI). The latter zwitterionic pair at the ends of an oligo(phenylethynylene) (OPE) chain has indeed been shown to be theoretically promising[12] and experimentally accessible.[4,13] The theoretical study of the **4B** and **4B′** models and the challenge to synthesize the corresponding tetraphenyl homologues **4b** and **4b′** were simultaneously launched in 2003 (Scheme 4).[12] The results are reported below.

Treatment of the totally dissymmetric dimethoxy[6]pericyclynetetrol **3b** with $SnCl_2$/HCl in dioxane/diethyl ether at 0 °C followed by hydrolytic treatment with 1 M NaOH led to a dark-violet residue, which was then purified by chromatography on silica gel. The polarity of the product required the addition of 1 % methanol to the eluting chloroform and the anisyl/pyridyl *carbo*-benzene **4b** was finally obtained in 16 % yield as a poorly soluble dark-red-violet solid (Scheme 5).

Several attempts at crystallization from chloroform afforded dark-red (almost black) lozenge-shaped plates or needles. As in the case of hexaphenyl-*carbo*-benzene **1a**, however, their weak diffracting power did not allow analysis by X-ray crystallography.

The ^{1}H NMR spectrum of highly diluted **4b** in a saturated $CDCl_3$ solution is quite complex, likely due to a high level of association. Nevertheless, all the characteristic signals are

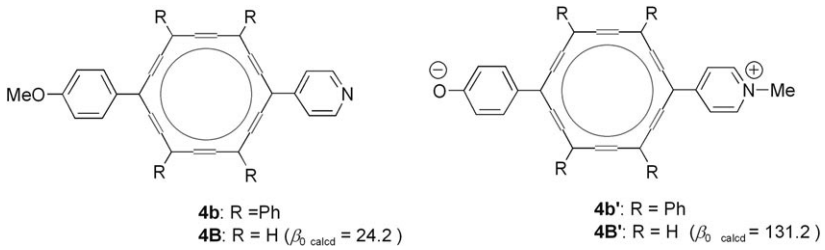

Scheme 4. Targeted donor/acceptor tetraphenyl-*carbo*-benzene chromophores **4b,b′** and their theoretical models **4B,B′** (geometries at the B3PW91/6-31G* level of theory, static quadratic hyperpolarizability β_0 given in 10^{-30} $cm^5 esu^{-1}$ units and calculated at the ZINDO/INDO-SOS level of theory).[12]

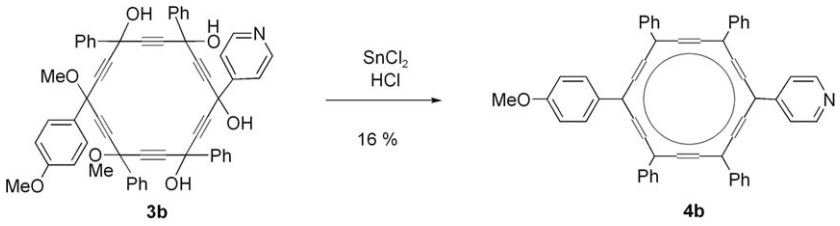

Scheme 5. Reductive aromatization of the *p*-anisyl-4-pyridylhexaoxy[6]pericyclyne **3b** to the corresponding donor/acceptor *carbo*-benzenic chromophore **4b**.

present and significantly deshielded with respect to those of the pericyclyne precursor **3b**. The OCH_3 signals occurring at $\delta = 3.60$–3.76 ppm in **3b** are thus shifted to 4.10–4.17 ppm in **4b**. The 2-C*H* signals of the 4-anisyl substituent are shifted from $\delta = 6.65$–6.77 ppm in **3b** to 7.35–7.50 ppm in **4b**. Beyond the complex resonances at $\delta =$ 7.60–7.95 ppm, assigned to other aromatic C*H* atoms, the 12 *ortho*-C*H* atoms of the aromatic substituents of the C_{18} ring (Ph, 4-Py, and 4-An) resonate at $\delta = 8.95$–9.10 and 9.15–9.23 ppm. Because of insufficient solubility, the ^{13}C NMR spectrum could not be recorded.

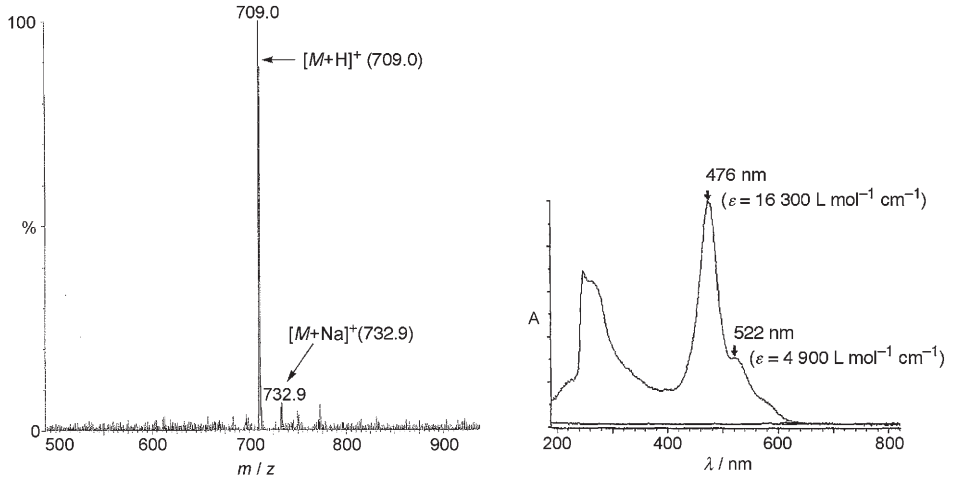

Figure 1. MALDI-TOF spectrum (left) and UV/Vis absorption spectrum (right) of the *p*-anisyl-4-pyridyltetraphenyl-*carbo*-benzenic chromophore **4b**.

The formula of **4b** was finally demonstrated by MALDI-TOF MS with the $[M+H^+]$ molecular peak at *m*/*z* 709 (Figure 1). The *carbo*-benzenic structure was confirmed by UV/Vis spectroscopy with characteristic absorptions at $\lambda_{max} = 476$ nm and $\lambda_{sh} = 522$ nm (Figure 1), which are similar to those of other hexaaryl-*carbo*-benzenes (e.g., for **1a**, $\lambda_{max} = 472$ nm, $\lambda_{sh} = 515$ nm).

An attempt to convert **4b** into the zwitterionic regioisomeric chromophore **4b′** (Scheme 4) was hampered by insolubility problems. Preliminary electric-field-induced second-harmonic (EFISH) measurement of the hyperpolarizability of the weak push–pull chromophore **4b** was, however, performed[14] and the synthesis of **4b** provides a basis for the future development of nonlinear optical applications of *carbo*-benzenic chromophores.

Dialkynyltetraphenyl-carbo-*benzene* ***4c*** *from* ***3c***: Until recently, only three kinds of groups could be anchored to the *carbo*-benzene ring: aryls (in **1a–d** and **4b**), tertiary alkyls (*t*Bu in **1c**), and hydrogen (**1d**,[7] **4d**,**e**: see below). None of these groups allows for further selective functionalization at the periphery of the C_{18} ring. In particular, although direct electrophilic substitution at CH vertices could be a priori envisioned by analogy with the Friedel–Craft chemistry of the benzene ring, theoretical studies based on the electron localization function (ELF) analysis predict that the edge sp carbon atoms of the C_{18} ring are more nucleophilic than the vertex sp^2 carbon atoms:[15] In the parent *carbo*-benzene **1**, the ELF nucleophilicity index (NI) is 0.87 for the sp carbon atoms, whereas it is only 0.69 for the sp^2 carbon atoms.[16] Unless the favored sp carbon adduct was kinetically unproductive (which is unlikely, at least with respect to polymerization), the electrophilic substitution of the sp^2 CH vertices should not compete (Scheme 6).

To circumvent this problem, the proton can be made intrinsically acidic by "*carbo*-merization" of the vertex sp^2 C–H bond: the corresponding ethynyl-substituted *carbo*-benzene should lend itself to selective peripheral electrophilic

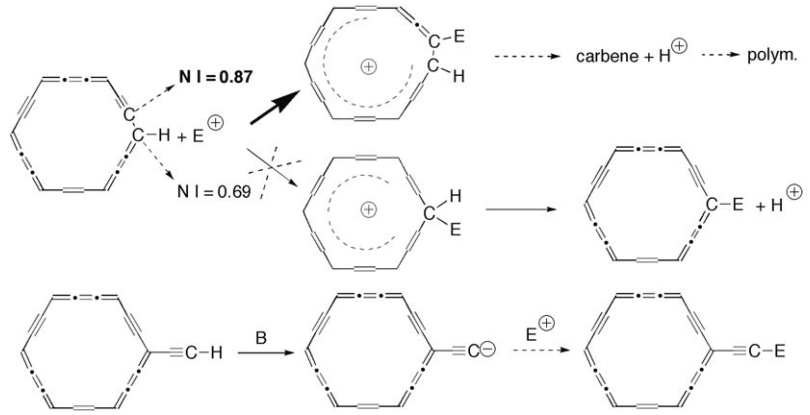

Scheme 6. Theoretically supported speculations on the alternative ways to achieve electrophilic substitution at the periphery of the *carbo*-benzene ring. NI represents the calculated ELF nucleophilicity index at either the edge sp carbon atoms or the vertex sp^2 carbon atoms of the C_{18} ring (the NIs are actually calculated over the C_{sp}–C_{sp} and C_{sp^2}–C_{sp} valence basins).[15,16]

substitution. Finally it must be emphasized that the compatibility of the ethynyl substituents at the *carbo*-benzene ring is a prerequisite for the synthesis of the long-sought total *carbo*-mer of benzene **1′** (Scheme 1).[1,9]

A "*para*"-dialkynyl *carbo*-benzene (with idealized D_{2h} symmetry) has been devised from the tetramethoxy[6]pericyclynediol **3c**.[10] Reductive aromatization of **3c** with $SnCl_2$/HCl required quite a long reaction time (6 h at room temperature). After mild hydrolytic treatment with saturated $NaHCO_3$ (the classical use of sodium hydroxide would cleave the C–Si bonds) and chromatography on silica gel, the *carbo*-benzene **4c** was isolated as a dark-violet solid in 10% yield (Scheme 7). The improved solubility provided by the $SiMe_3$ termini of **4c** (relative to **1a** and **4b**) facilitated full spectroscopic characterization.

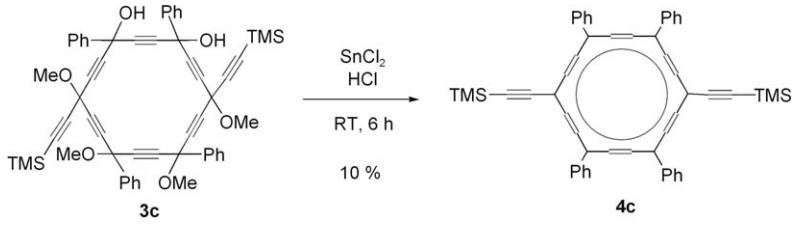

Scheme 7. Reductive aromatization of tetramethoxy[6]pericyclynediol **3c** to the "*para*"-dialkynyl *carbo*-benzene **4c** (TMS: trimethylsilyl).

The matrix-assisted laser desorption/ionization time-of-flight (MALDI-TOF) mass spectrum displays characteristic peaks at *m*/*z* 741.1 ($[M+Na]^+$) and 719.2 ($[M+H]^+$). The presence of peripheral triple bonds is confirmed by the IR absorption of their stretching vibration (2149 cm^{-1}). The phenyl-substituted *carbo*-benzenic ring is evidenced from the electronic spectrum by characteristic absorptions at $\lambda_{max}=472$ nm and $\lambda_{sh}=513$ nm.

The ^1H NMR spectrum of **4c** displays characteristic signals shifted to a much lower field than the corresponding signals in the pericyclyne precursor **3c.** The macrocyclic diatropic ring current exerts its deshielding effect as far away as 5 Å from the ring (through five bonds): The $SiCH_3$ protons of **4c** resonate at $\delta=0.66$ ppm, whereas those of **3c** do so at $\delta=0.21$ ppm. The phenyl C*H* resonances are typical of a *carbo*-benzene environment: $\delta=7.70$, 7.91, and 9.44 ppm for the *p*-C*H*, *m*-C*H*, and *o*-C*H* signals, respectively (the corresponding signals from **3c** resonate at $\delta=7.32$–7.37 ppm for *p*- and *m*-C*H* and at $\delta=7.66$–7.74 for *o*-C*H*).[10]

Full assignment of the ^{13}C NMR spectrum of **4c** (including its quaternary carbon atoms) could also be achieved from the long-range ^1H-^{13}C HMQC spectrum, recorded in the presence of an activator of T_1 relaxation ($[Cr(acac)_3]$).[17]

Single crystals of **4c** deposited from chloroform were suitable for an X-ray diffraction analysis (Figure 2). The C_{18} ring exhibits a quasi-D_{6h} symmetry with average $C_{sp}\cdots C_{sp}$ and $C_{sp}\cdots C_{sp^2}$ bond lengths of 1.22 and 1.38 Å, respectively. The bond angles in the C_{18} ring are similar to those reported for the X-ray crystal structure of **1a** or calculated at the DFT level of theory for other *carbo*-benzene derivatives (see below). The phenyl substituent planes are only slightly tilted from the C_{18} mean plane (ca. 4.9–14.4°). Co-crystallized chloroform molecules induce an elongation disorder of the external triple bonds whose lengths are intermediate between 1.24 and 1.05 Å (the apparent shortening of the average length of the triple bonds to ca. 1.15 Å can be considered as an artifact; this has previously been discussed on the basis of an electron compression effect to which X-ray diffraction is sensitive).[18] The chloroform–**4c** interaction is preserved in solution as indicated by the shift in the absorption bands of this solvent to $\tilde{\nu}=2360$ and 2341 cm^{-1} in the IR spectrum of **4c**.

Deprotection of the external triple bonds of **4c** was attempted. Treatment of **4c** with tetrabutyl ammonium fluoride (TBAF) in THF at −78°C induced an intense color change (from light to dark violet), but hydrolysis after 10 min afforded polymeric material only. When the reaction time was limited to 1 min prior to hydrolysis, the NMR spectrum of the soluble material (after extraction and evaporation) showed all the signals compatible with the expected diethynyl-*carbo*-benzene structure **4c′** (Scheme 8, Figure 3): $\delta=4.32$ (s; ≡C-*H*), 7.68 (t; *p*-C*H*), 7.96 (t; *m*-C*H*), 9.44 ppm (d; *o*-C*H*). Chromatography on silica gel did not allow isola-

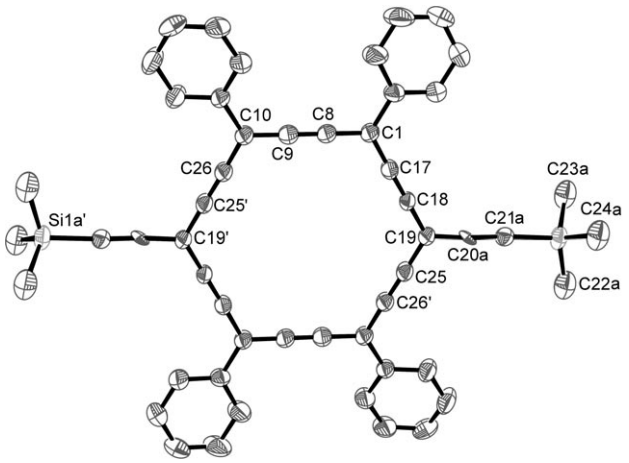

Figure 2. ORTEP diagram of the X-ray crystal structure of dialkynyltetraphenyl-*carbo*-benzene **4c** ($R_1 = 0.0691$). Selected bond distances and bond angles are listed in Table 7.

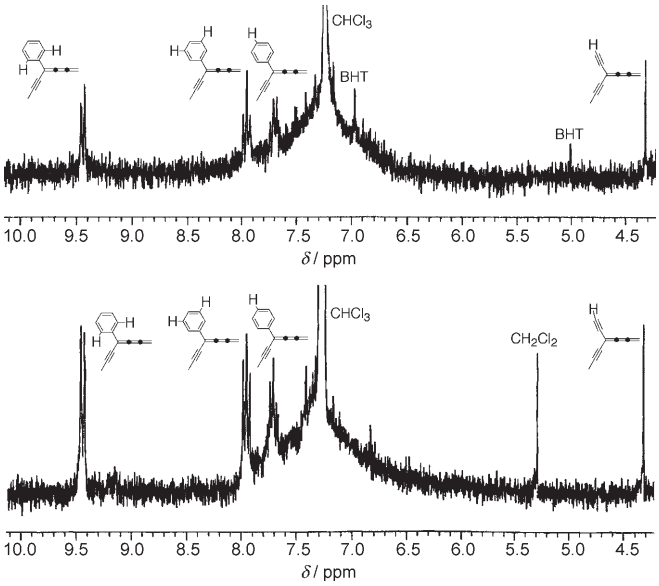

Figure 3. ^{1}H NMR spectra of diethynylhexaphenyl-*carbo*-benzene **4c′** as a mixture with polymeric material and other identified impurities (CH_2Cl_2, BHT), as produced by two different methods. Top: Desilylation of *carbo*-benzene **4c** (top Scheme 8). Bottom: Desilylation of pericyclyne **3c** to **3c′** followed by reductive aromatization of **3c′** (bottom Scheme 8).

tion of **4c′** in the pure state. On the other hand, attempts to improve the selectivity of the reaction by using other desilylation procedures (K_2CO_3/MeOH,[19] MeLi[20]) were unsuccessful.

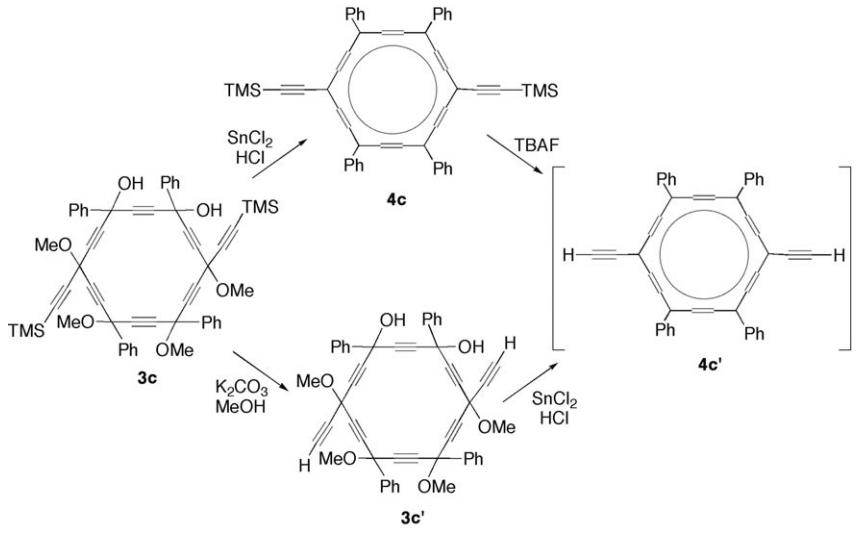

Scheme 8. Two possible methods to access diethynyltetraphenyl-*carbo*-benzene **4c′** from the hexaoxy[6]pericyclyne **3c**.

Desilylation of the dialkynylhexaoxy[6]pericyclyne **3c** prior to aromatization was then envisioned (Scheme 8). Reaction of **3c** with K_2CO_3 in a methanol/THF mixture thus afforded the bis-terminal diethynylpericyclynediol **3c′**, which was then treated with 10 equiv of $SnCl_2$ in ethereal HCl at $-20/+20$ °C, with or without a co-solvent (H_2O, AcOH), with or without ultrasound activation, and for various reaction times (5 min–5 h). After hydrolytic treatment with $NaHCO_3$, a few of the ^{1}H NMR spectra of the crude material displayed the same four signals as those obtained after treatment of **4c** with TBAF. In all cases, however, these signals were of low intensity relative to the broad signals assigned to the polymeric materials. The best result was obtained with the classical $SnCl_2$/HCl/Et_2O system, by starting the reaction at -20 °C, continuing at 0 °C for 15 min before hydrolysis, and direct chromatography of the organic phase without evaporation. The NMR spectrum of the fraction corresponding to the nonpolar orange TLC spot is shown in Figure 3. Although further purification was not possible, superimposition of the spectra obtained by both methods (TBAF + **4c** and $SnCl_2$/HCl + **3c′**) confirms their assignment to structure **4c′**. The assignment was further confirmed by DFT calculations (B3LYP/6-31+G**), which indeed predict an unusual deshielding of the acetylenic proton of **4c′** ($\delta_{calcd} = 4.48$ ppm vs. $\delta_{calcd} = 4.32$ ppm).

Tetraphenyl-carbo-*benzene* ***4d*** *from* ***3d***: The synthesis of nonsubstituted *carbo*-benzene **1** remains a challenge. The *carbo*-benzene ring is surely stabilized by substitution with aryl or tertiary alkyl groups, but its viability with unsubstituted CH vertices remains to be determined. The sole re-

ported example of an incompletely substituted *carbo*-benzene is **1d**, in which the ("*meta*") CH vertices are nonadjacent, that is, they are "protected" by alternation with *p-tert*-butylphenyl substituents: whatever the Kekulé form of **1d**, all the butatrienic edges are trisubstituted. In contrast, in *carbo*-benzene **1**,[4] all the butatriene edges are only disubstituted and it is unclear whether global aromaticity is able to overcome the intrinsic fragility of such units (Scheme 9). The first question is thus whether Kekulé forms containing a disubstituted butatriene edge are viable: This question was addressed by attempting to synthesize the tetraphenyl-*carbo*-benzene **4d** in which the ("*ortho*") CH vertices are adjacent (Scheme 9).

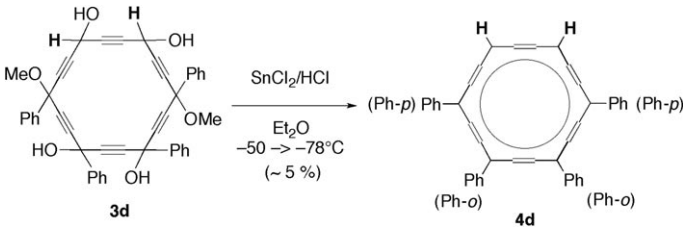

Scheme 10. Reductive aromatization of a hexaoxy[6]pericyclynediol to tetraphenyl-*carbo*-benzene with "*ortho*" CH vertices. The two types of chemically nonequivalent phenyl substituents are denoted as *o*-Ph *and p*-Ph, for which the equivalent representatives occupy "*ortho*" and "*para*" positions at the *carbo*-benzene ring, respectively.

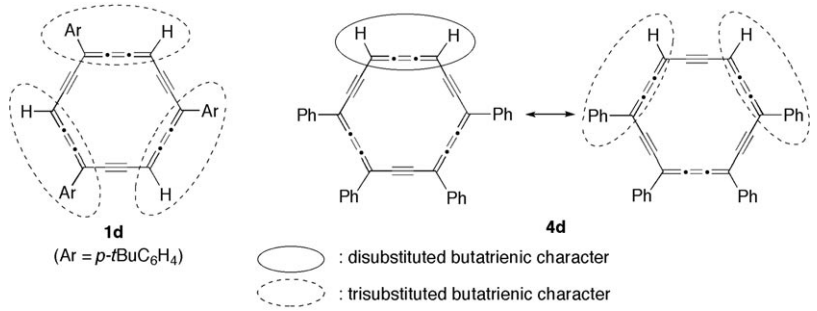

Scheme 9. Comparison of the minimal substitution level of the 50% butatrienic edges in known **1d** and targeted **4d** *carbo*-benzene derivatives.

According to the pioneering report,[7b] conversion of hexaoxy[6]pericyclyne **2d** with three nonadjacent secondary carbinol vertices to the partially substituted *carbo*-benzene **1d** required milder conditions than did the reaction with hexasubstituted **2a–c**.[10] Aromatization of the tetraphenyl[6]pericyclynetetrol **3d**, possessing two adjacent secondary carbinol vertices, turned out to be even more problematic. Treatment of **3d** with $SnCl_2$/HCl under various conditions, hydrolytic treatment, extraction, and evaporation to dryness of the red-orange organic layers brought about decomposition to yield insoluble black residues. It was finally found that treatment of **3d** with $SnCl_2$/HCl in diethyl ether between −78 and −50 °C for 1 h, followed by immediate deposition and elution of the crude solution on a preparative-TLC plate, allowed collection of the expected product **4d** as a red-violet solid (Scheme 10).

The presence of the phenyl-substituted *carbo*-benzene ring is evidenced from the electronic spectrum by absorptions at $\lambda_{max}=442$ nm and $\lambda_{sh}=491$ nm. The ipsochromic shift observed for **4d** relative to the absorptions of **1a**, **1b**, **4b**, and **4c**, and the bathochromic shift relative to those of **1c** and **1d**, are consistent with the relative extent of radial conjugation: Over four conjugated π-electron-rich substituents in **4d**, instead of six in **1a**, **1b**, **4b**, and **4c** ($\lambda_{max}=472$–479 nm and $\lambda_{sh}=513$—522 nm) and three in **1c** and **1d** ($\lambda_{max}=424$–427 nm and $\lambda_{sh}=468$—475 nm).[7b]

The ^{1}H NMR spectrum ($CDCl_3$, 250 MHz, 20 °C) of **4d** displays the expected highly deshielded signals of the *p*-, *m*-, and *o*-C*H* nuclei of the phenyl substituents at around $\delta=7.77$, 8.05, and 9.55 ppm, respectively; the "*ortho*" C*H* nuclei of the *carbo*-benzene ring resonate as a singlet at $\delta=9.70$ ppm. The latter value is close to the chemical shift of the "*meta*" C*H* nuclei of the *carbo*-benzene ring in **1d** ($\delta=9.87$ ppm in $CDCl_3$).[7b] This basic assignment is also confirmed by excellent agreement with the chemical shifts calculated at the B3LYP/6-31+G** level of theory (see also Figure 12 and Table 5). At 400 MHz, improved resolution of the *p*-, *m*-, and *o*-C*H* signals and ^{1}H-^{1}H COSY correlation allow for separate assignment of the nonequivalent phenyl substituents Ph-1 and Ph-2 (Figure 4). It is however not possible at this stage to unequivocally assign Ph-1 and Ph-2 to the nonequivalent pairs of chemically equivalent phenyl substituents *o*-Ph and *p*-Ph at the "*ortho*" and "*para*" positions of the *carbo*-benzene ring, respectively (Scheme 10). This problem will be tackled with the aid of theoretical calculations (see below).

A ^{13}C NMR spectrum was recorded at 100 MHz. Despite the dilution, all the *C*H signals were unambiguously assigned. In particular, the unsubstituted *C*H vertex nuclei resonate at $\delta=89.6$ ppm, a value close to the chemical shift of the corresponding carbon atoms in **1d** ($\delta=86.6$ ppm). Weak signals were also tentatively assigned to the quaternary carbon atoms by resorting to a comparison with the proposed assignment for related environments in **1a** and **1d**.[7b] The assignment is also in quite good agreement with the ^{13}C chemical shifts calculated for **4d** at the B3LYP/6-31+G** level of theory (see below and Figure 13).

Single dark red crystals of **4d** deposited from deuterated chloroform solution were submitted to X-ray diffraction analysis (Figure 5). Despite a slight distortion of around 4° towards a "flat chair" conformation, the C_{18} ring of **4d** is quasiplanar. The planes of the four phenyl substituents are all tilted in the same direction by an angle ranging from 14 to 18° from the C_{18} ring mean plane (16.5° on average). To

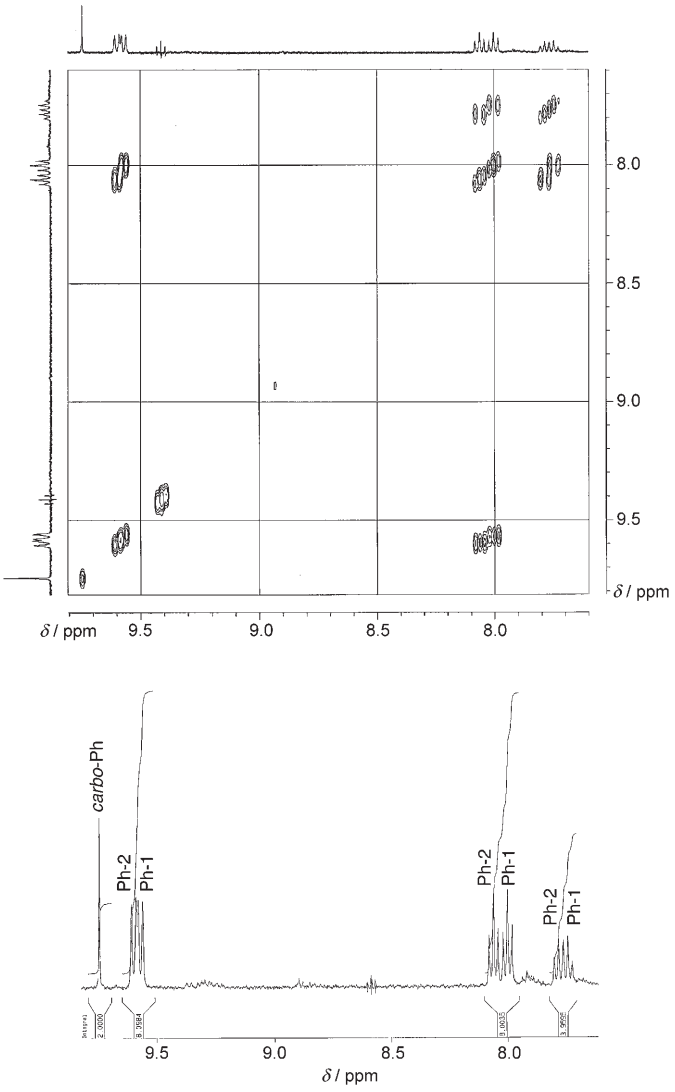

Figure 4. ^{1}H NMR spectra of tetraphenyl-*carbo*-benzene **4d** ($CDCl_3$, 400 MHz): Integration and assignment (top) and ^{1}H-^{1}H COSY-45 correlation (bottom).

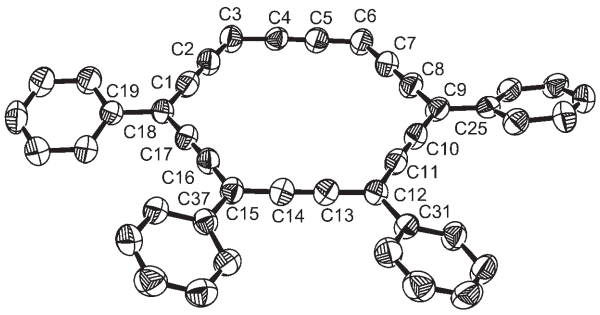

Figure 5. ORTEP diagram of the X-ray crystal structure of tetraphenyl-*carbo*-benzene **4d** ($R_1 = 0.0754$). Selected bond distances and bond angles are listed in Table 8.

gain an insight into the exact values of the structural parameters, the structure of **4d** has been refined by calculations at the B3PW91/6-31G** level of theory: The results are detailed below, where they are compared with those concerning the optimized structures of **1** (without a phenyl substituent) and **1a** (with six phenyl substituents).

In the crystal, molecules of **4d** are stacked along the *a* axis. The C_{18} rings are almost aligned above each other, thus forming columns of a quasi-regular hexagonal section with a diameter of around 7 Å. As in the cases of **4c** and **1a**,[7b] chloroform molecules are co-crystallized. In the case of **4d**, $CDCl_3$ molecules are intercalated between successive C_{18} rings of a given column. Their refinement indicate two types of interactions (Figure 6): Hydrogen bonds between the deuterium atoms and the C_{18} π system[21] and a quasi van der Waals contact near the C_{18} ring center between the chlorine atoms of two successive disordered, but refined, $CDCl_3$ molecules (Cl···Cl ≈3.88 Å vs. $r_{vdW}(Cl) = 1.84$ Å).[22] In such carbon-rich π systems, the channel arrangement and haloform doping might induce interesting conducting properties.[23]

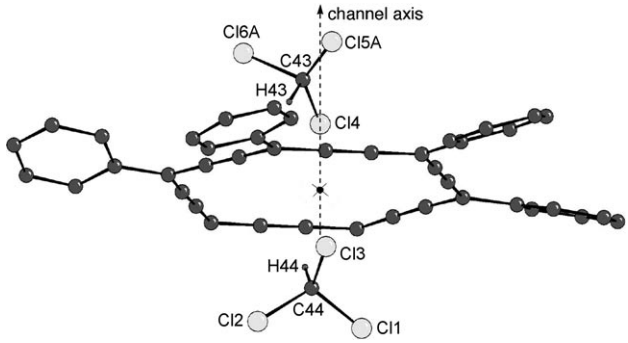

Figure 6. Interacting $CDCl_3$ molecules inside channels of C_{18} rings in the crystal structure of **4d**. The disordered, but refined, intermolecular Cl(13)···Cl(14) van der Waals contact (≈3.88 Å) occurs near the centroid of the C_{18} ring (marked by a cross).

*Attempted reductive aromatization of tetramethoxy[6]pericyclynediols **3e** and **3g***: Attempts to treat diphenyltetramethoxy[6]pericyclynediol **3g** with $SnCl_2$/HCl did not afford any evidence for the formation of diphenyl-*carbo*-benzene **4g** (with four adjacent CH vertices, Scheme 2). Likewise, attempts at controlled reduction of the tetraphenyl[6]pericyclynedione **3f** did not afford the tetraphenyl-*carbo*-benzoquinone **4f** (Scheme 2) nor the corresponding tetraphenyl-*carbo*-hydroquinone **4f'**.[24]

Similar treatment of tetraphenyltetramethoxy[6]pericyclynediol **3e** at 0 °C for 35 min, followed by chromatography, gave minute quantities of a dark red solid whose NMR analysis ($CDCl_3$, 250 MHz) indicated the likely presence of the "*para*" isomer of **4d**, namely **4e** (Figure 7). Characteristic signals at $\delta = 7.74$ (t), 7.97 (t), 9.52 (d), and 9.87 ppm (s) could indeed be assigned to the *p*-C_6H, *m*-C_6H, *o*-C_6H, and $C_{18}H$ nuclei, respectively. The latter value, in particular, is similar to the chemical shift of the $C_{18}H$ nuclei of **4d** ($\delta =$ 9.70 ppm) and **1d** ($\delta = 9.87$ ppm).[7b]

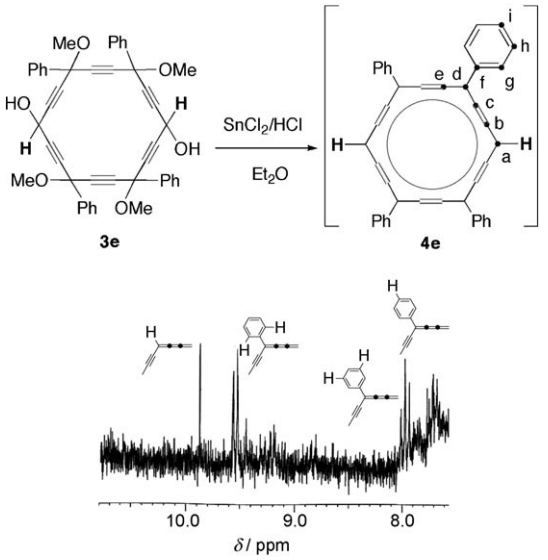

Figure 7. Top: Reductive aromatization of a tetramethoxy[6]pericyclynediol to tetraphenyl-*carbo*-benzene with "*para*" CH vertices; nonequivalent carbon nuclei are numbered a–i (used in Figure 8 and Table 1). Bottom: First ^{1}H NMR spectrum ($CDCl_3$, 250 MHz) of the product obtained after conducting the reaction at 0 °C. Beside broad signals assigned to polymeric materials, the four sharp aromatic signals were tentatively assigned to those of **4e**, on the basis of a comparison with the NMR spectra of **4d** and **1d**.[7b]

Treatment of **3e** with $SnCl_2$/HCl at a lower temperature (from −25 to −10 °C for 2.5 h) followed by hydrolysis with 2 M sodium hydroxide and chromatography on silica gel afforded **4e** as the major component as a violet solid. Further purification of **4e** was not possible, but it could be identified by MALDI-TOF mass spectrometry (*m*/*z* 526.25, $[M]^+$) and fully characterized by NMR techniques. The ^{1}H NMR spectrum confirmed the interpretation of the preliminary results (Figure 7). The ^{13}C NMR spectrum was recorded in the presence of an activator of T_1 relaxation ($[Cr(acac)_3]$),[17] allowing complete assignment by ^{1}H-^{13}C correlation (Figure 8). The HSQC (heteronuclear single-quantum correlation) spectrum first allowed identification of all the tertiary carbon nuclei (*C*H). In particular, the *C*H carbon atoms of the C_{18} ring resonate at $\delta = 88.16$ ppm, in the same range as the corresponding *C*H carbon atoms of **4d** (see above) and **1d**.[7b] The HMBC (heteronuclear multiple-bond correlation) spectrum finally allowed the identification of all the quaternary carbon nuclei and the assignment of most of them (Table 1).

The three signals at $\delta = 123.1$, 120.2, and 116.3 ppm globally correspond to carbon atoms {b, c, e}. The intensities of the HMBC spots do not allow a direct assignment, but comparison with the ^{13}C assignment for **1d** and **4d** (see below) and use of the linear correlation of Figure 14 suggest an assignment in the given order (Table 1).

Direct comparison between theory and experiment for phenyl-substituted *carbo*-benzenes 1a and 4d: The existence of the "naked" *carbo*-benzene **1** was proposed in 1995[1] and

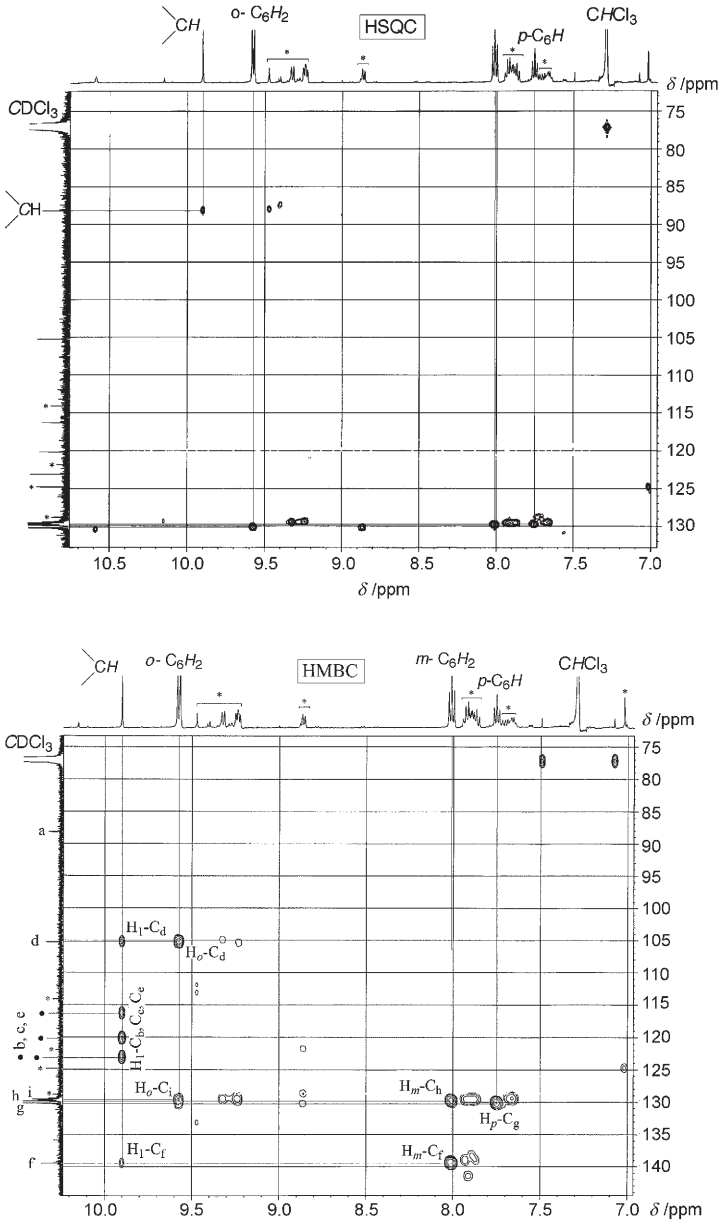

Figure 8. HSQC ($^{1}J_{C\text{-}H}$, top) and HMBC ($^{N}J_{C\text{-}H}$, N > 1, bottom) spectra (125 MHz, $CDCl_3$) of tetraphenyl-*carbo*-benzene **4e** as a mixture with an undetermined side-product likely containing one deshielded proton (δ = 9.47 ppm) and four nonequivalent phenyl groups (asterisked signals: *).

at the same time the syntheses of aryl-substituted derivatives were reported.[7a] The intrinsic "aromatic" nature of the C_{18} ring (in particular its D_{6h} symmetry) was then predicted by DFT calculations performed on the naked parent molecule **1**.[3] The DFT method used (B3PW91/6-31G**) was validated by indirect comparison with the geometry of the C_{18} ring of the hexaphenyl derivative **1a** published in 1998 (HF and semi-empirical calculations predicted a "wrong" localized D_{3h} symmetry).[3b,e] Very recently, calculations were also performed on the "total" *carbo*-mer of benzene **1′** ($C_{30}H_6$, Scheme 1), which, however, also remains an unknown molecule.[9] Direct comparison of experimentally known substi-

Table 1. Assignment of the ^{13}C NMR chemical shifts of tetraphenyl-*carbo*-benzene **4e** from ^{1}H-^{13}C HSQC and HMBC spectra (125 MHz, $CDCl_3$; Figure 8). The vertical correspondence for the {b, c, e} nuclei is not proven, but inferred from theoretical analysis (see next section on **4d** and also Figure 14).

Carbon atom[a]	a	{b	c	e}	d	f	g	h	i
$\delta_{^{13}C}$	88.2	{123.1	120.2	116.3}	105.3	139.5	130.2	129.9	129.5

[a] For the carbon labeling see Figure 7.

tuted *carbo*-benzenes with their calculated structures had to be performed. The selected representatives **1a** and **4d** are structurally related to the parent molecule **1** through complete and partial phenyl substitution, respectively. Their structures calculated at the B3PW91/6-31G** level of theory have been compared with their X-ray crystal structures. The effects of phenyl substitution on the apparent aromaticity of the C_{18} macrocycle are discussed below in terms of structural, magnetic, and energetic criteria.

Structural criterion of the aromaticity of phenyl-substituted carbo-*benzenes*: The experimental (X-ray) and calculated (DFT) structural parameters of variously phenyl-substituted *carbo*-benzenes $C_{18}H_{6-n}Ph_n$ ($n=0$: **1**; $n=4$: **4d**; $n=6$: **1a**) are compared below. To facilitate comparison, a common labeling is adopted (Scheme 11).

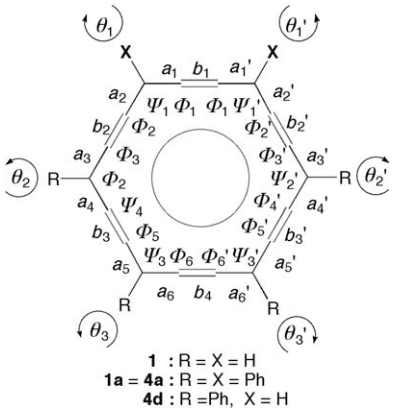

Scheme 11. Common labeling of structural parameters (used in Tables 2 and 3) for phenyl-substituted *carbo*-benzenes $C_{18}H_{6-n}Ph_n$ ($n=0$, 4, 6). a_i, a_i' and b_i, b_i' denote the spC–sp^2C and spC–spC bond lengths, respectively; Ψ_i, Ψ_i' and Φ_i, Φ_i' denote the spC-sp^2C-spC and spC-spC-sp^2C bond angles, respectively; θ_i, θ_i' denote the tilting (dihedral) angles between the phenyl planes and the mean plane of the C_{18} ring.

Hexaphenyl-*carbo*-benzene **1a**: Two conformational states **1a′** and **1a″** of $C_{18}Ph_6$ were first calculated under the D_{6h} symmetry constraint, with the six phenyl substituents either coplanar or perpendicular to the plane of the C_{18} ring, respectively. The planar form **1a′** and the orthogonal form **1a″** exist as seven- and six-order saddle points, respectively, on the potential energy surface. The normal modes of the imaginary frequencies correspond to the rotation of the phenyl substituents. The planar **1a′** and orthogonal **1a″** are higher in energy than the minimum energy structure **1a** by 6.5 and 33.1 kcal mol^{-1}, respectively (Figure 9, Scheme 11). The latter exhibits no overall symmetry because of the variable tilting (17–20°) of the phenyl planes with respect to the plane of the central C_{18} ring. This tilting can be regarded as a trade

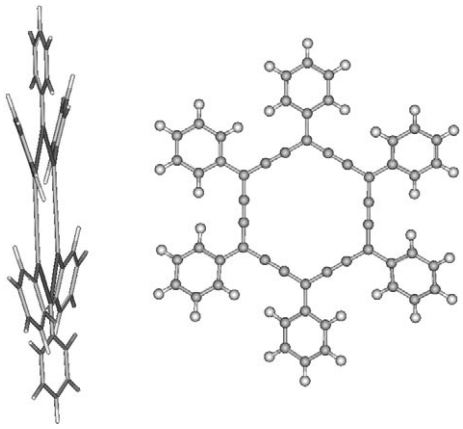

Figure 9. Front and side view of the optimized structure of hexaphenyl-*carbo*-benzene **1a** at the B3PW91/6-31G** level of theory (see Table 2).

off between van der Waals repulsion of facing *ortho*-hydrogen atoms (lying only 1.957 Å from each other in **1a′**) and residual conjugation of the nonhybridized p atomic orbitals (AOs) of the carbon atoms of the phenyl substituents with those of the C_{18} macrocycle. Comparison of the relative energies of **1a′** and **1a″** with respect to the equilibrium structure of **1a** (Figure 9) shows that despite the energetic cost of the van der Waals repulsion in the non-orthogonal forms **1a** and **1a′** (which vanishes in the orthogonal form **1a″**), the energetic benefit of complete or partial conjugation of the phenyl substituents in **1a** and **1a′** (which also vanishes in **1a″**) is a determining factor (see below). Nevertheless, the geometry of the D_{6h} symmetric C_{18} ring of the parent nonsubstituted *carbo*-benzene **1** is almost unperturbed relative to **1a**.

Tetraphenyl-*carbo*-benzene **4d**: The agreement between the experimental (X-ray) and calculated (DFT) structures of **4d** is excellent (see Table 2 and Table 3). Despite the lower chemical symmetry, the C_{18} ring in the optimized geometry of **4d** is almost perfectly planar. This suggests that the slight distortion observed in the X-ray diffraction analysis of **4d** (see above) is due to crystal packing. In the DFT structure, the planes of the phenyl rings adjacent to the nonsubstituted vertices of the macrocycle are tilted by 11.5°, whereas the two next ones are tilted by 20.2 and 20.5° (Figure 10). As in the case of **1a**, this tilting results from the van der Waals repulsions between facing *ortho*-hydrogen atoms of adjacent phenyl substituents. The corresponding H–H distance in the optimized geometry is about 2.5 Å, that is, about twice the van der Waals radius of the hydrogen atom.[22]

Table 2. Experimental and selected calculated geometrical parameters for variously phenyl-substituted *carbo*-benzenes **1a**, **4d**, and **1**.[a]

	$<a>$	$<b>$	$<a_1>$	b_1	$<a_6>$	b_4	$<\theta>$	$<\theta_3>$	$<\Psi>$	$<\Psi_1>$	$<\Psi_3>$	$<\Phi>$	$<\Phi_1>$	$<\Phi_6>$
1a (X-ray)	1.391	1.217	–	–	–	–	na	–	118.7	–	–	na	–	–
1a (calcd)[b]	1.380	1.236	–	–	–	–	18.6	–	118.9	–	–	179.0	–	–
4d (X-ray)	–	–	1.373	1.226	1.391	1.232	–	16.2	–	122.6	118.6	–	177.9	179.3
4d (calcd)[b]	–	–	1.366	1.240	1.381	1.235	–	20.3	–	123.0	119.3	–	178.9	178.3
1 (calcd)[b]	1.369	1.239	–	–	–	–	–	–	122.6	–	–	178.7	–	–
1 (calcd)[c]	1.366	1.233	–	–	–	–	–	–	122.6	–	–	178.7	–	–
1 (calcd)[d]	1.374	1.243	–	–	–	–	–	–	122.7	–	–	178.7	–	–
1 (calcd)[e]	1.377	1.249	–	–	–	–	–	–	122.7	–	–	178.7	–	–

[a] Labeling is given in Scheme 11. Experimental data for **1a** have been extracted from ref. [7b]. Bond distances are in Å, bond and phenyl-C_{18} tilting angles are in degrees. The average uncertainties in the bond distances and angles determined by using X-ray diffraction analysis are approximately ± 0.01 Å and $\pm 0.1°$, respectively. $<x>$ denotes the arithmetic mean of the parameters x. [b] At the B3PW91/6-31G** level of theory. [c] B3PW91/6-311+G**. [d] BP86/6-311+G**. [e] BP86/6-31G**.

Table 3. Comparison of experimental and selected geometrical data for tetraphenyl-*carbo*-benzene **4d** calculated at the B3PW91/6-31G** level of theory.[a]

	$<a_1>$	b_1	$<a_2>$	$<b_2>$	$<a_3>$	θ_2	θ_3	θ_3'	θ_2'	$<\Psi_1>$	$<\Psi_2>$	$<\Phi_1>$
4d (X-ray)	1.373	1.226	1.350	1.230	1.375	16.8	14.3	18.1	15.1	122.6	118.6	177.9
4d (calcd)	1.366	1.240	1.372	1.237	1.379	11.5	20.5	20.2	11.5	123.0	118.6	178.9

[a] Labeling is given in Scheme 11. Bond distances are in Å, bond and phenyl-C_{18} tilting angles are in degrees. $<x>$ denotes the arithmetic mean of the parameters x.

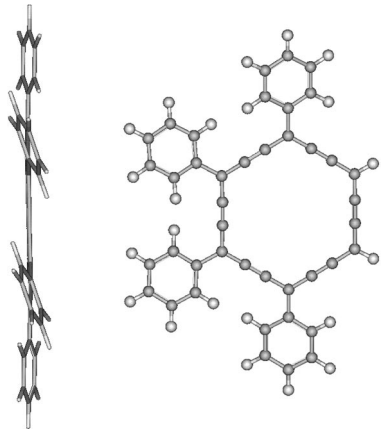

Figure 10. Front and side view of the optimized structure of tetraphenyl-*carbo*-benzene **4d** at the B3PW91/6-31G** level of theory (see Tables 2 and 3).

The substitution pattern of **4d** can be regarded as a 33:67 hybrid of **1** (two adjacent CH vertices) and **1a** (four adjacent CPh vertices). And indeed, the local geometry of both types of edges HC···C···C···CH and PhC···C···C···CPh in **4d** is very similar to those of **1** and **1a**, respectively. At "high" levels of calculation (B3PW91/6-31G** or/6-311+G**), the C–C bond lengths and valence angles at the hydrogen-substituted vertices of the C_{18} ring of **4d** become virtually identical to those of **1** (Table 2). Note, however, that the BP86 functional with the same basis set leads to slightly longer bonds (Table 2). The best level of theory formally appears to be B3PW91/6-311+G**, which has a higher computational cost than B3PW91/6-31G**. However, owing to the intrinsic uncertainty of the bond lengths determined by using X-ray diffraction analyses (± 0.01 Å on average), the quality of the results at the B3PW91/6-31G** level of theory definitely validate the corresponding calculation method hitherto used for the study of *carbo*-benzene derivatives.[4]

More globally, the geometry of the C_{18} ring is not markedly influenced by the symmetry or the extent of phenyl-substitution (at least in **1**, **1a**, **4d**, and in **4c** as well). This can be summarized by stating that the C_{18} ring of *carbo*-benzene derivatives possesses an intrinsic structural aromatic character just as does the parent C_6 ring of benzene derivatives.

Energetic criterion of the aromaticity of phenyl-substituted carbo-*benzenes*: The stability of the *carbo*-benzene derivative with regard to its high degree of unsaturation is the experimental indication that the C_{18} ring is energetically aromatic. More rigorously, the energetic aromaticity of **1** has been demonstrated both in the geometrical Hückel–Dewar sense (the minimum energy structure is attained by symmetrization of a given cyclic conjugation path) and in the topological Breslow sense (the minimum energy structure is attained by cyclization of the conjugation path with respect to a reference acyclic one).[4] In the early empirical sense, however, aromaticity is the energy-dictated propensity of molecules containing a cyclically unsaturated ring to preserve this structural unit upon chemical transformations (e.g., substitution is favored over addition).

In **1a** and **4d**, π-electronic delocalization can spread out over the peripheral phenyl substituents, but the "independency" of the *carbo*-benzenic unit has already been evidenced by the preservation of its local structure, whatever the

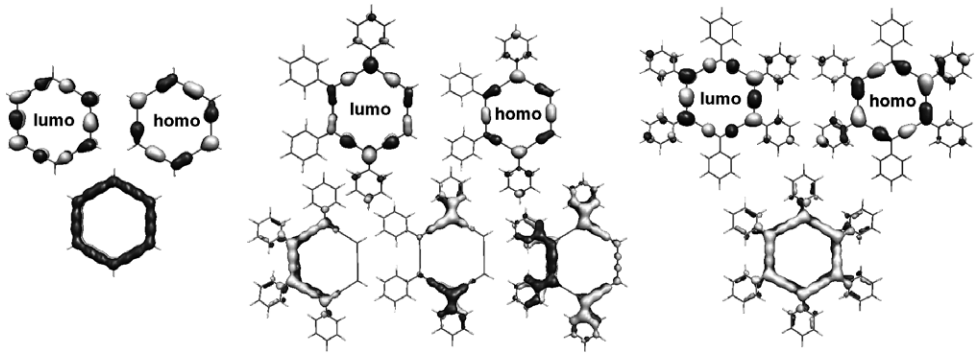

Figure 11. Frontier and lowest π_z MOs of unsubstituted *carbo*-benzene **1** (left), the tetraphenyl *carbo*-benzene **4d** (middle), and the hexaphenyl-*carbo*-benzene **1a** (right) derivatives. Energies of the MOs calculated at the B3PW91/6-31G** level of theory are presented in Table 4.

degree of phenyl substitution (see above). The analysis of the energetic aromaticity criterion of the *carbo*-benzenic ring is now refined by comparison of their π-MO systems.

Because of the tilting of the phenyl substituents, the frontier and lowest π_z MOs of **1a** and **4d** are similar to those of **1**. The frontier orbitals remain mainly located over the C_{18} ring (Figure 11 and Table 4). Only the HOMO of **1a** and the lowest π MOs of **4d** partly extend to the phenyl substituents (in **4d**, the tilting angle of "*para*"-phenyl substituents is indeed lowered to 11.5° because of the absence of van der Waals repulsion with the adjacent C–H vertices; see Table 2). Although structural and magnetic criteria indicate that the aromaticity of **1a** and **4d** is slightly lowered relative to that of unsubstituted *carbo*-benzene **1** (see Table 2), the peripheral conjugation is reflected by the decrease in size of the HOMO–LUMO gap (Figure 11 and Table 4).

Table 4. Comparison of the frontier and lowest π_z MOs of unsubstituted *carbo*-benzene **1** with the tetraphenyl **4d** and hexaphenyl **1a** derivatives calculated at the B3PW91/6-31G** level of theory. The MOs are ranked by increasing order of their eigenvalues given in hartrees [a.u.].

1	**4d**	**1a**
Gap:	Gap:	Gap:
2.932 eV ≡ 0.10773 a.u.	2.381 eV ≡ 0.08749 a.u.	2.338 eV ≡ 0.08592 a.u.
MO 58: −0.10640	MO 138: −0.10887	MO 178: −0.10807
MO 57: −0.21413	MO 137: −0.19636	MO 177: −0.19399
MO 43: −0.39255	MO 105: −0.39434	MO 133: −0.40569
	MO 104: −0.40093	
	MO 103: −0.40577	

Magnetic criterion of the aromaticity of phenyl-substituted carbo-*benzenes*: The nuclear magnetic shielding tensors of **1a** and **4d** were calculated at the B3LYP/6-31+G** level of theory (GIAO formalism) from static equilibrium structures. The ^{1}H and ^{13}C NMR chemical shift values were obtained after averaging the isotropic magnetic shielding of experimentally equivalent nuclei on the NMR timescale (293 K).

^{1}H NMR chemical shifts: The agreement between experimental and calculated ^{1}H chemical shifts is satisfactory (Table 5). Calculated chemical shifts of ^{1}H nuclei located in the vicinity of the C_{18} ring (C*H* vertices and *o*-C_6H_2) are, however, shifted downfield by around 1 ppm compared with experimental values: This is consistent with the sensitive specific effect of a strong diatropic circulation around the C_{18} ring.

Closer inspection shows that for each compound, the experimental and calculated ^{1}H NMR chemical shifts of the phenyl substituents are more accurately correlated. For **1a**, the correlation is perfectly linear (Figure 12). For **4d**, possessing nonequivalent pairs of phenyl substituents *o*-Ph and *p*-Ph (Scheme 10), the exact correlation is a priori more difficult to establish. It can, however, be assumed that the calculated relative shielding of the *meta* and *para* protons (remote from the C_{18} ring) of *o*-Ph and *p*-Ph is satisfactory (their absolute shielding lies in the "classical" range). An excellent linear correlation is then also afforded (Figure 12). This allows the tentative assignment of the correlated substituents Ph-1 and Ph-2 (Figure 4) to *p*-Ph and *o*-Ph (Scheme 10), respectively.

^{13}C NMR chemical shifts: The available experimental and calculated ^{13}C NMR chemical shifts of **1a** and **4d** are listed and tentatively assigned in Figure 13. The assignment of the

Table 5. Comparison of the ^{1}H NMR chemical shifts of **1a** and **4d** calculated at the B3LYP/6-31+G** level of theory with the experimental values obtained from this work ($CDCl_3$, 400 MHz).[a]

	4d (exptl)	**4d** (calcd)	**1a** (exptl)[b]	**1a** (calcd)
ortho ^{1}H (phenyl)	Ph-1: 9.57 Ph-2: 9.60	*p*-Ph: 10.31 *o*-Ph: 10.24	9.45 (9.49)	10.56
meta ^{1}H (phenyl)	Ph-1: 8.00 Ph-2: 8.06	*p*-Ph: 8.21 *o*-Ph: 8.31	7.99 (8.01)	8.18
para ^{1}H (phenyl)	Ph-1: 7.74 Ph-2: 7.78	*p*-Ph: 7.87 *o*-Ph: 7.94	7.72 (7.74)	7.78
^{1}H (C_{18} ring)	9.74	10.95	–	–

[a] Chemical shifts are in ppm with respect to tetramethylsilane. The given values have been averaged, assuming a rapid exchange through 180° ring flips of the phenyl substituents and a pseudo-D_{6h} and pseudo-C_{2v} symmetry for **1a** and **4d**, respectively. For definitions of the Ph-1 and Ph-2 substituents, see Figure 4. For definitions of the *o*-Ph and *p*-Ph substituents, see Scheme 10. [b] Values reported in ref. [7b] are given in parentheses.

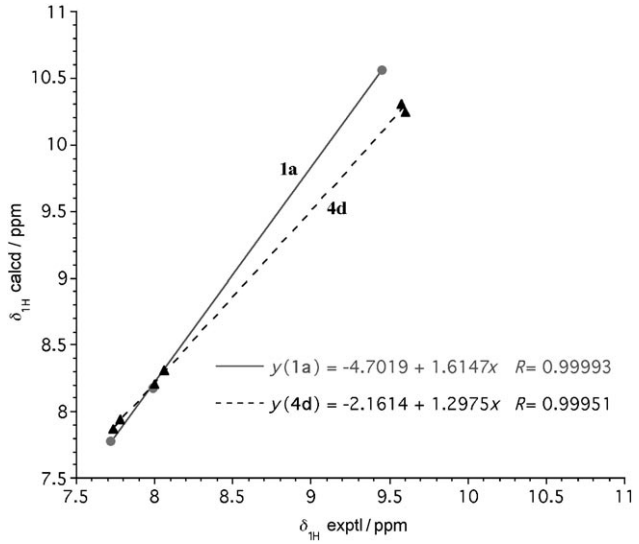

Figure 12. Correlation between experimental ($CDCl_3$, 400 MHz) and calculated (B3LYP/6-31+G**) ^{1}H chemical shifts of the phenyl substituents of **1a** and **4d** (Table 5). The COSY-correlated Ph-1 chemical shifts are assigned to those of the "*para*" equivalent phenyl substituents *p*-Ph, while the COSY-correlated Ph-2 chemical shifts are assigned to those of the "*ortho*" equivalent phenyl substituents *o*-Ph (see Figure 4 and Scheme 10).

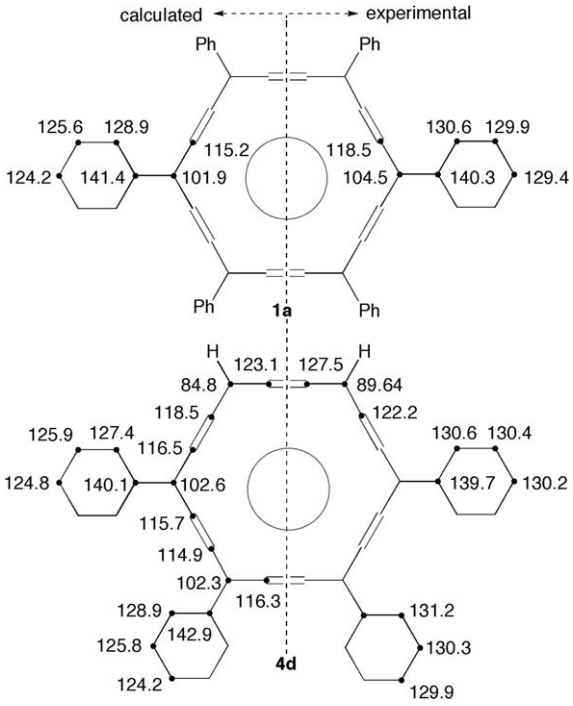

Figure 13. Calculated (B3LYP/6-31+G**, left) and experimental ($CDCl_3$, 293 K, right) ^{13}C NMR chemical shifts of **1a** and **4d**.[7b] Chemical shifts are given in ppm with respect to tetramethylsilane. The calculated values have been averaged, assuming a rapid exchange through 180° ring flips of the phenyl substituents and a pseudo-D_{6h} and pseudo-C_{2v} symmetry for **1a** and **4d**, respectively.

experimental values is supported by an excellent general correlation (Figure 14). For **4d**, as a result of dilution, only

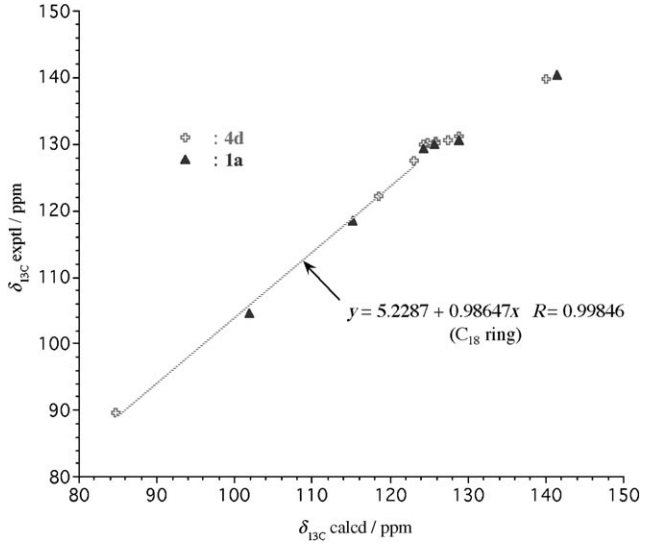

Figure 14. General correlation between calculated (B3LYP/6-31+G**) and experimental ^{13}C NMR chemical shifts of **1a** and **4d** for the assignment depicted in Figure 13. The dotted line represents a linear correlation restricted to the ^{13}C nuclei of the C_{18} rings of both **1a** and **4d**.

three types of quaternary carbon atoms could be detected: The correlation suggests that weak signals at $\delta = 122.2$ and 127.5 ppm actually correspond to the sp carbon atoms attached to the CH vertices. The correlation presents two distinct parts, corresponding to the phenyl carbon atoms (top right) and the C_{18} ring carbon atoms (bottom left), respectively. The linear fit over the C_{18} ring part allows prediction of the chemical shifts of the sp and sp^2 ^{13}C nuclei of the C_{18} ring, which could not be unambiguously detected in the NMR spectrum of **4d** (see equation in Figure 14).

The consistency of the above analyses provides further proof of the structures of **1a** and **4d** in solution. It also allows exact assignment of the ^{13}C NMR chemical shifts to the {b, c, e} carbon atoms of **4e**, the "*para*" regioisomer of **4d** (see above and also Figure 8 and Table 1).

Nucleus independent chemical shifts (NICS): As demonstrated by von R. Schleyer et al.,[25] the NICS values at the center of unsaturated rings are relevant indices of their magnetic aromaticity. They have been calculated for **1a** and **4d** at the B3LYP/6-31+G** level of theory by using either experimental or re-optimized geometries. All the values proved to be strongly negative (Figure 15): −13.5 ppm for **1a** and −14.8 ppm for **4d** (to be compared with −17.9 ppm for **1**).[3a,b] Their relative values are discussed in the next section and compared with the structural aromaticity indices $\sigma_r(d)$.

In conclusion, both NICS and ^{1}H NMR chemical shifts show the existence of strong diatropic circulation around the C_{18} ring regardless of the phenyl substitution pattern. The *carbo*-benzene ring is therefore strongly magnetically aromatic and more so than the benzene ring (for benzene at the B3LYP/6-31+G* level of theory: NICS = −8.0 ppm, $\delta_{^1H} = 7.3$ ppm).[3b,4]

Correlation between structural and magnetic aromaticity of phenyl-substituted *carbo*-benzenes: Katritzky's factor analysis showed that the general aromaticity concept is two dimensional:[26] The orthogonal factors correspond to the "classical" (structural–energetic) criterion on one hand and to the magnetic criterion on the other. von R. Schleyer et al. later showed that, in restricted ranges of structures, the two aromaticity factors are actually correlated.[27] The aromaticity of rings containing sp carbon atoms has been much less studied, but Katritzky's and von R. Schleyer's statements likely remain valid: This has definitely been shown over an extended series of *carbo*$_k$-[3]radialenic derivatives ($k=0$, 1, 2).[28] This has been further illustrated for a restricted range of phenyl-substituted *carbo*-benzenes **1**, **1a**, and **4d**. The NICS value at the centroid of the C_{18} ring was selected as a measure of the magnetic criterion (contrary to ^{1}H NMR chemical shifts, it is homogeneously defined for all three derivatives). The root-mean-square (rms) deviation from the average endocyclic C–C bond length $\sigma_r(d)$ was selected as a structural measure of the classical criterion. Values are listed in Figure 15. Despite the minimum number of points (three), the linear correlation is noteworthy.

	NICS [ppm]	$\sigma_r(d)$ [Å]
1a (calcd structure)	–13.5	0.068
4d (calcd structure)	–14.8	0.066
4d (exptl structure)	–15.0	0.066
1	–17.9	0.061
1 (B3PW91/6-311+G**)	-	0.063
1 (BP/6-311+G**)	-	0.062
1 (BP/6-31G**)	-	0.060

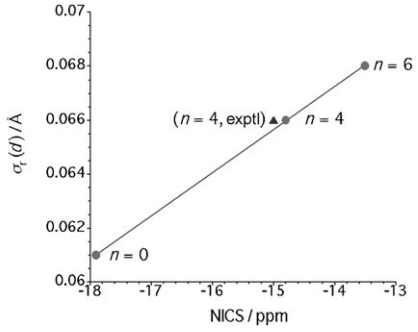

Figure 15. Comparison of structural ($\sigma_r(d)$, B3PW91/6-31G**, unless otherwise noted) and magnetic (NICS, B3LYP/6-31+G**) aromaticity indices for phenyl-substituted *carbo*-benzenes $C_{18}Ph_nH_{6-n}$, $n=0$ (**1**), 4 (**4d**), and 6 (**1a**). $\sigma_r(d)=\{1/18\,(d_i-<d>)^2\}^{1/2}$, where d_i denotes the length of the ith C–C bond in the C_{18} macrocycle ($1\le i\le 18$), and $<d>$ the corresponding mean bond length. The graph illustrates the correlation between the structural and magnetic aromaticity indices.

Conclusion

Ten years after the conceptual proposition and the first experimental achievements,[6,7a] the scope of *carbo*-benzene chemistry has been expanded to new horizons from the standpoints of synthetic methodology and substitution compatibility.[29] Whereas the theoretical aromaticity of the *carbo*-benzene ring has been extensively demonstrated and analyzed for fictitious representatives of maximal symmetry ($C_{18}R_6$: R = H, C≡CH),[3,4,9] empirical aromaticity has now been established for real representatives with various substitution patterns. In particular, the possibility of alkynyl substitution provides a firm basis for the a posteriori functionalization of *carbo*-benzenic bricks. Indeed, whereas the electrophilic substitution of sp^2 C–H vertices has been predicted to be poorly selective (according to ELF analysis), terminal acetylenic substituents should be relatively acidic enough to lend themselves to selective oxidative or isohypsic coupling reactions, including dehydropolymerization. Desilylation of the protected derivative **4c** to the bis-terminal derivative **4c′** (or direct synthesis of the latter) needs to be improved, but efforts in this direction are in progress.[30]

These exploratory efforts were motivated by the desire to push forward the frontiers of the aromaticity realm. Aromaticity is a concept underlying so many applied properties that it still instigates acute debates regarding its physicochemical significance.[31] It has been shown here that radial conjugation with more than three phenyl substituents just plays an auxiliary role in the stabilization and in the macrocyclic symmetry perturbation of the *carbo*-benzenic structures. The unsubstituted *carbo*-benzene **1** remains to be synthesized, but the proven compatibility of two adjacent ("*ortho*") nonsubstituted CH vertices in **4d** allows us to be optimistic.

More practically, the synthesis of *carbo*-benzene derivatives proceeds with satisfactory efficiency until the penultimate step, giving the key hexaoxy[6]pericyclyne substrate.[10] The last step, based on the use of the $SnCl_2$/HCl system, however, remains problematic (low yields and high sensitivity to the substrate structure). Optimization of the reductive aromatization procedure is the next practical challenge.

Experimental Section

General: All reagents were used as commercially available. THF and diethyl ether were dried and distilled over sodium/benzophenone, pentane and dichloromethane over P_2O_5. Commercial solutions of EtMgBr were 3 M in diethyl ether, those of *n*BuLi were 1.6 or 2.5 M in hexane and their effective concentrations were checked by titration with 2,2,2′-trimethylpropionanilide.[32] The hexaoxy[6]pericyclynes **3a–g** were prepared as previously described.[10] All reactions were carried out under nitrogen or argon using Schlenk and vacuum line techniques. Column chromatography was carried out on silica gel (60 Å, 70–200 μm). Silica gel thin-layer chromatography (TLC) plates (60F254, 0.25 mm) were revealed by treatment with an ethanolic solution of phosphomolybdic acid (20%). The following analytical instruments were used. IR: Perkin-Elmer GX FT-IR spectrometer, 0.1 mm CaF_2 cell. ^{1}H and ^{13}C NMR: Bruker AC 200, WM 250, DPX 300, or AMX 400 spectrometer. X-Ray diffraction: IPds STOE diffractometer. Mass spectrometry: Quadrupolar Nermag R10-10H spectrometer. Elemental analyses: Perkin-Elmer 2400 CHN (flash combustion and detection by catharometry). All IR and NMR spectra were recorded in $CDCl_3$ solutions. IR absorption frequencies $\tilde{\nu}$ are in cm^{-1}. NMR chemical shifts δ are in ppm, with positive values to high frequency

relative to the tetramethylsilane reference; coupling constants J are in Hz.

Crystallographic and structural parameters for 4c (Figure 2, Tables 6 and 7): X-ray crystallographic structure data were collected on a Stoe Imaging Plate Diffraction System (IPDS) equipped with an Oxford Cryosystems Cryostream Cooler Device using graphite-monochromated $Mo_{K\alpha}$ radiation. The final unit cell parameters were obtained by means of a least-squares refinement of a set of well-measured reflections and crystal decay was monitored during data collection; no significant fluctuations in intensity were observed. The structures were solved by direct methods using the SIR92 program[33] and refined by least-squares procedures on F^2 with SHELXL-97.[34] All hydrogen atoms were located on a difference Fourier map, but introduced and refined by using a riding model. All non-hydrogen atoms were anisotropically refined.

Crystallographic and structural parameters for 4d (Figure 5, Tables 6 and 8): X-ray crystallographic structure data were collected at a low temperature on a STOE one-circle Imaging Plate detector System CCD equipped with an Oxford Cryosystems Cryostream Cooler Device. Diffractometer settings: tube power = 1.50 kW; tube voltage = 50 kV; tube current = 30 mA; collimator size = 0.5 mm; detector distance = 70.0 mm; 2θ range = 2.9–48.4°; $d(hkl)$ range = 14.228–0.867 Å; φ movement mode = rotation; φ start/end/increments = 0.0/200.2/1.4°; no. of exposures = 143; irradiation/exposure = 6.00 min; measurement duration = 24 h; extinction coefficient = 0.002(3). Crystal decay was monitored and no fluctuations in the intensity were observed during data collection. Final unit cell parameters were obtained by the least-squares refinement of sets of well-measured reflections. The structure was solved by using direct methods with the aid of the SIR92 program[31b] and refined by least-squares procedures on F^2 using SHELXL-97.[35] All hydrogen atoms were located on a difference Fourier maps, but were introduced in calculation in idealized positions with isotropic thermal parameters fixed at 20% higher than those of the carbon atoms to which they are connected. All non-hydrogen atoms were anisotropically refined. Least-squares refinement was carried out by minimizing the function $w(F_o-F_c)^2$, where F_o and F_c are the observed and calculated structure factors. A weighting scheme was used in the last refinement cycles for which the weights were calculated from the following expression: $w=[\text{weight}][(1-\Delta F)/6\sigma F]^2$. Models reached convergence with $Rw=[\Sigma w(|F_o|-|F_c|)^2/\Sigma(|F_o|)^2]^{1/2}$ (expression of ponderation: weight = $1/[2(F_o^2)+(0.1312P)^2]$). For a satisfactory complete analysis, the ratio of the rms shift to standard deviation has to be less than 0.1 with no significant features in the final difference maps. Two chlorine atoms of a molecule of solvent ($CHCl_3$) were found statistically disordered at two sites and were refined with a ratio of occupancy equal to 0.5. Calculations were

Table 6. Crystallographic data for **4c** and **4d**.

	4c	**4d**
formula	$C_{26.25}H_{19}Cl_{0.375}Si$ ($=C_{52}H_{38}Si_2\cdot(CHCl_3)_{0.25}$)	$C_{42}H_{22}\cdot(CHCl_3)_2\cdot(H_2O)_{1/2}$
M_r	375.80	774.34
T [K]	180	180(2)
λ [Å]	0.71073	0.71073
crystal system	orthorhombic	triclinic
space group	*Pbnb*	$P\bar{1}$
unit cell dimensions		
a [Å]	13.569(5)	9.5892(11)
b [Å]	17.636(5)	13.2921(16)
c [Å]	18.205(5)	16.882(2)
α [°]	90	67.579(13)
β [°]	90	88.863(15)
γ [°]	90	70.119(13)
V [Å^3]	4357(2)	1855.5(4)
Z	8	2
ρ_{calcd} [mg m^{-3}]	1.146	1.386
μ [mm^{-1}]	0.161	0.496
$F(000)$	1575	790
crystal size [mm]	0.45 × 0.35 × 0.3	0.25 × 0.22 × 0.10
crystal description	–	red prism fragment
θ range [°]	2.20–24.71	2.33–24.24
index ranges	$-15\le h\le 15$	$-11\le h\le 11$
	$-20\le k\le 20$	$-15\le k\le 15$
	$-21\le l\le 20$	$-19\le l\le 19$
reflns collected/	28523/3713	11960/5531
unique	[R(int) = 0.0576]	[R(int) = 0.0556]
completeness [%]	99.7 (2θ = 24.71°)	92.4 (θ = 24.24°)
absorption correction	semi-empirical from equivalents	refdelf (DIFABS)[a]
max/min transmission	0.948/0.936	0.345/0.766
data/restraints/ params	3713/6/282	5531/15/479
GOF on F^2	0.984	0.920
final R indices	R_1 = 0.0691	R_1 = 0.0754
[$I>2\sigma(I)$]	wR_2 = 0.1886	wR_2 = 0.1863
R indices	R_1 = 0.0902	R_1 = 0.1491
(all data)	wR_2 = 0.2070	wR_2 = 0.2314
largest diff. peak/ hole [e Å^{-3}]	0.956/−0.447	0.424/−0.448

[a] See ref. [40].

Table 7. Bond lengths [Å] and angles [°] for **4c**.

C1−C17	1.381(4)	C20b−C21b	1.05(6)
C1−C8	1.383(5)	C21a−Si1a	1.859(19)
C8−C9	1.220(5)	C21b−Si1b	1.89(6)
C9−C10	1.393(5)	Si1a−C24a	1.848(15)
C10−C26	1.380(5)	Si1a−C22a	1.843(7)
C17−C18	1.226(5)	Si1a−C23a	1.846(7)
C18−C19	1.383(4)	Si1b−C24b	1.85(2)
C19−C25	1.376(5)	Si1b−C22b	1.853(15)
C19−C20a	1.385(16)	Si1b−C23b	1.843(14)
C19−C20b	1.58(3)	C25−C26′	1.225(5)
C20a−C21a	1.24(3)	C26−C25′	1.225(5)
C17-C1-C8	118.4(3)	C20a-C19-C18	124.1(5)
C9-C8-C1	179.2(4)	C25-C19-C20b	127.3(9)
C8-C9-C10	178.8(4)	C18-C19-C20b	111.6(9)
C26-C10-C9	118.1(3)	C21a-C20a-C19	175.5(11)
C18-C17-C1	178.4(4)	C20a-C21a-Si1a	176.0(12)
C17-C18-C19	177.4(4)	C21b-C20b-C19	172(3)
C25-C19-C20a	114.7(5)	C26′-C25-C19	177.2(4)
C25-C19-C18	121.1(3)	C25′-C26-C10	177.7(3)

Table 8. Bond lengths [Å] and angles [°] for **4d**.

C1−C2	1.221(8)	C9−C10	1.381(8)
C1−C18	1.386(8)	C10−C11	1.228(8)
C2−C3	1.355(9)	C11−C12	1.379(8)
C3−C4	1.379(8)	C12−C13	1.392(8)
C4−C5	1.226(8)	C13−C14	1.232(8)
C5−C6	1.366(8)	C14−C15	1.389(8)
C6−C7	1.344(9)	C15−C16	1.367(9)
C7−C8	1.238(9)	C16−C17	1.214(8)
C8−C9	1.363(8)	C17−C18	1.387(9)
C2-C3-C4	122.7(6)	C3-C4-C5	177.6(7)
C7-C6-C5	122.5(5)	C4-C5-C6	178.2(6)
C11-C12-C13	118.8(5)	C9-C10-C11	179.1(7)
C16-C15-C14	118.4(5)	C12-C13-C14	179.6(7)
C1-C18-C17	118.7(5)	C8-C9-C10	118.4(5)
C1-C2-C3	178.5(7)		

performed by using the WinGX program, version 1.64 04,[36] and drawings of molecules were realized with the aid of ORTEP32.[37] Atomic scattering factors were taken from *International Tables for X-ray Crystallography*.[38]

CCDC-637831 (**4c**) and CCDC-637832 (**4d**) contain the supplementary crystallographic data for this paper. These data can be obtained free of charge from The Cambridge Crystallographic Data Centre via www.ccdc.cam.ac.uk/data_request/cif.

The reliability factor of the present structure (7.54%) could be lowered slightly by further refinement (to 6.93%), but at the expense of a systematic increase in the estimated standard deviation of bond distances (by up to 0.003 Å) and angles (by up to 0.1°). The present structure was thus selected for the purpose of comparison with DFT-calculated geometries (see the section on Structural criterion above).

Synthetic procedures

1,4,7,10,13,16-Hexaphenylcyclooctadeca-1,2,3,7,8,9,13,14,15-nonaen-5,11,17-triyne (hexaphenyl-*carbo*-benzene 1a, 4a): *From **3a***: A solution of hexayne **3a** (49 mg, 0.06 mmol) in Et_2O (2 mL) was treated with $SnCl_2{\cdot}2H_2O$ (135 mg, 0.6 mmol) and saturated ethereal HCl (4 mL) at 0°C for 10 min. Stirring was then continued at RT for 15 min. After dilution with Et_2O and addition of aqueous NaOH (1 M, 3 mL), the organic layer was washed with brine, dried with $MgSO_4$, and concentrated under reduced pressure. Chromatography on silica gel ($CHCl_3$) gave **4a** as a dark-violet solid (7 mg, 22%). The compound was identified from its ^{1}H NMR spectrum and by comparison with previously reported data.[7b] ^{1}H NMR ($CDCl_3$, 250 MHz): $\delta = 7.72$ (t, $^3J_{HH} = 7.5$ Hz, 6H; *p*-C_6H), 7.99 (t, $^3J_{HH} = 7.5$ Hz, 12H; *m*-C_6H_2), 9.45 ppm (d, $^3J_{HH} = 7.5$ Hz, 12H; *o*-C_6H_2). *From **3a′***: A solution of hexayne **3a′** (58 mg, 0.07 mmol) in Et_2O (3 mL) was treated with $SnCl_2{\cdot}2H_2O$ (1.58 g, 7 mmol) and saturated ethereal HCl (10 mL) at 0°C for 10 min. Stirring was then continued at RT for 35 min. After dilution with Et_2O and addition of aqueous NaOH (1 M, 5 mL), the organic layer was washed with brine, dried with $MgSO_4$, and concentrated under reduced pressure. Chromatography on silica gel ($CHCl_3$) gave **4a** as a dark-violet solid (6 mg, 12%). The compound was identified from its ^{1}H NMR spectrum and by comparison with previously reported data.[7b]

4-[10-(4-Methoxyphenyl)-4,7,13,16-tetraphenylcyclooctadeca-1,2,3,7,8,9,13,14,15-nonaene-5,11,17-triynyl]pyridine (*p*-anisyl-4-pyridyl-tetraphenyl-*carbo*-benzene 4b): A solution of hexayne **3b** (28 mg, 0.033 mmol) in Et_2O (1 mL) was treated with $SnCl_2{\cdot}2H_2O$ (75 mg, 0.33 mmol) and a dioxane solution of HCl (4 M, 4.7 mL, 18.8 mmol) at 0°C for 2 h. The mixture was allowed to warm up to RT over a 15 min period and then stirring was continued for another 30 min. After treatment with aqueous NaOH (1 M) and extraction with a THF/Et_2O mixture, the organic layer was washed with brine, dried with $MgSO_4$, and concentrated under reduced pressure. Chromatography on silica gel ($CHCl_3$ + 2% MeOH) gave **4b** as a poorly soluble dark-violet solid (4 mg, 16%). $R_f \approx 0.26$ ($CHCl_3$); M.p. >400°C; ^{1}H NMR (250 MHz, $CDCl_3$): $\delta = 4.10$–4.17 (m, 3H; CH_3O-C_6H_4), 7.35–7.50, 7.60–7.95, 8.95–9.10, 9.15–9.23 ppm (four complex multiplets, 28H; aromatic C*H*); IR (KBr): very complex spectrum; UV ($CHCl_3$): λ_{max} (ε [L mol^{-1} cm^{-1}]) = 248 (11125), 262 (sh, 10492), 476 (16280), 522 (sh, 4859), 572 nm (sh, 1825) (Figure 1); MS (MALDI-TOF, positive mode, DMSO, matrix: TCNQ, NaI): *m*/*z*: 732 $[M+Na]^+$, 709 $[M+H]^+$ (Figure 1).

1,10-Bis(2-trimethylsilylethynyl)-4,7,13,16-tetraphenylcyclooctadeca-1,2,3,7,8,9,13,14,15-nonaene-5,11,17-triyne (*p*-bis(trimethylsilylethynyl)-tetraphenyl-*carbo*-benzene 4c): A solution of octayne **3c** (364 mg, 4.2 mmol) in Et_2O (20 mL) was treated with $SnCl_2{\cdot}2H_2O$ (787 mg, 4.2 mmol) and a dioxane solution of HCl (4 M, 15 mL, 62 mmol) at 0°C for 15 min. The mixture was allowed to warm up to RT over a 15 min period and stirring was then continued for 6 h. After treatment with a saturated aqueous $NaHCO_3$ solution and extraction with a mixture of THF/Et_2O, the organic layer was washed with brine, dried with $MgSO_4$, and concentrated under reduced pressure. Chromatography on silica gel ($CHCl_3$) gave **4c** as a dark-violet solid (28 mg, 10%). $R_f \approx 0.77$ ($CHCl_3$); M.p. 224°C; ^{1}H NMR (250 MHz, $CDCl_3$): $\delta = 0.66$ (s, 18H; $Si(CH_3)_3$), 7.70 (t, $^3J_{HH} = 7$ Hz, 4H; *p*-C_6H), 7.91 (t, $^3J_{HH} = 7$ Hz, 8H; *m*-C_6H_2), 9.44 ppm (d, $^3J_{HH} = 7$ Hz, 8H; *o*-C_6H_2); ^{13}C{^{1}H} NMR (100 MHz, $CDCl_3$): $\delta = 0.51$ ($Si(CH_3)_3$), 78.61 ($Me_3SiC{\equiv}C$), 104.95 ($Me_3SiC{\equiv}C$-*C*), 105.07 (Me_3Si-*C*≡C), 105.71 (Ph-*C*), 115.39, 119.05, 122.09 (spC of the C_{18} ring), 130.23 (*m*-*C*H of Ph), 130.46 (*p*-*C*H of Ph), 130.55 (*o*-*C*H of Ph), 139.48 ppm (*ipso*-*C* of Ph); IR ($CDCl_3$): $\tilde{\nu} = 2958$, 2927 (C–H), 2149 (C≡CSi), 1599, 1495, 1434 (phenyl C=C), 1261 cm^{-1} (C–Si); UV/Vis ($CHCl_3$): λ_{max} (ε [L mol^{-1} cm^{-1}]) = 469 (20246), 472 (sh, 20176), 513 (8697), 532 (4976), 562 nm (sh, 1180); MS (MALDI-TOF, positive mode, DMSO, matrix: 1,8-dihydroxyanthrone, NaI): *m*/*z*: 741 $[M+Na]^+$, 719 $[M+H]^+$, 718 $[M]^+$.

Single crystals deposited from $CDCl_3$ were submitted to an X-ray diffraction analysis (Figure 2, Tables 6 and 7).

1,10-Diethynyl-4,7,13,16-tetraphenylcyclooctadeca-1,2,3,7,8,9,13,14,15-nonaene-5,11,17-triyne (*p*-diethynyltetraphenyl-*carbo*-benzene 4c′): A solution of octayne **3c′** (90 mg, 0.123 mmol) in Et_2O (1 mL) was treated with $SnCl_2{\cdot}2H_2O$ (277 mg, 1.23 mmol) and a dioxane solution of HCl (4 M, 2 mL, 8 mmol) at −20°C for 10 min. Stirring was then continued for 15 min at 0°C. After treatment with a saturated aqueous $NaHCO_3$ solution at 0°C, the organic layer was diluted with CH_2Cl_2 (3 mL) and washed with H_2O. Direct chromatography on silica gel (heptane/EtOAc 8:2) of the concentrated organic layer (before evaporation to dryness) gave a dark-violet solid containing **4c′** as a mixture with polymeric material (7 mg, <10%). $R_f \approx 0.55$ (heptane/EtOAc 5:5); ^{1}H NMR (250 MHz; $CDCl_3$): $\delta = 4.32$ (s, 2H; ≡C-*H*), 7.71 (t, 4H; *p*-C*H*), 7.95 (t, 8H; *m*-CH_2), 9.42 ppm (d, 8H; *o*-CH_2).

1,4,7,10-Tetraphenylcyclooctadeca-1,2,3,7,8,9,13,14,15-nonaene-5,11,17-triyne ("*ortho*"-tetraphenyl-*carbo*-benzene 4d): A solution of hexayne **3d** (30 mg, 0.05 mmol) in Et_2O (1 mL) was treated with $SnCl_2{\cdot}2H_2O$ (105 mg, 0.5 mmol) and saturated ethereal HCl (3 mL) at −78°C. The mixture was allowed to warm up to −50°C over a 35 min period and stirring was then continued for another 20 min at this temperature. The solution was then directly deposited on a preparative TLC plate and eluted with hexane/EtOAc (8:2, then 5:5). An orange slice of silica was scraped off and extracted with $CHCl_3$. The solution was filtered through Celite and concentrated under reduced pressure to give **4d** (5 mg) as a dark-red solid. ^{1}H NMR ($CDCl_3$, 400 MHz): $\delta = 7.74$ (t, $^3J_{HH} = 7.4$ Hz, 2H; *p*-C_6H_2 Ph-1), 7.78 (t, $^3J_{HH} = 7.8$ Hz, 2H; *p*-C_6H_2 Ph-2), 8.00 (t, $^3J_{HH} = 7.7$ Hz, 4H; *m*-C_6H_5 Ph-1), 8.06 (t, $^3J_{HH} = 7.7$ Hz, 4H; *m*-C_6H_5 Ph-2), 9.57 (d, $^3J_{HH} = 7.3$ Hz, 4H; *o*-C_6H_5 Ph-1), 9.60 (d, $^3J_{HH} = 7.4$ Hz, 4H; *o*-C_6H_5 Ph-2), 9.74 ppm (s, 2H; $C_{18}H$). The separate assignment for each pair of equivalent phenyl substituents (Ph-1, Ph-2) was based on a COSY-45 correlation (Figure 4). ^{13}C{^{1}H} NMR ($CDCl_3$, 100 MHz): $\delta = 131.24$, 130.63, 130.42, 130.26 (*o*-, *m*-*C*H), 130.20, 129.93 (*p*-*C*H), 89.64 (C_{18} *C*H), 139.7 (*ipso*-*C*H), 127.2 (HC···*C*···*C*···CH), 122.2 ppm (HC···*C*···C···CPh); other very weak signals (remaining sp*C* of the C_{18} ring) could not be unambiguously identified; UV/Vis ($CHCl_3$): $\lambda_{max} = 442$ nm and $\lambda_{sh} = 491$ nm; MS (MALDI-TOF, positive mode, DMSO, matrix: 1,8-dihydroxyanthrone or TCNQ, NaI): *m*/*z* (%): 580 (100) $[M-C_2H+DMSO+H]^+$, 524 (82) $[M-C_2H+Na]^+$; this tentative interpretation is supported by a common primary fragmentation to $M-C_2H$; the secondary peak also corresponds to $[M-2H]^+$.

Single crystals deposited from $CDCl_3$ were submitted to an X-ray diffraction analysis (Figure 5).

1,4,10,13-Tetraphenylcyclooctadeca-1,2,3,7,8,9,13,14,15-nonaene-5,11,17-triyne ("*para*"-tetraphenyl-*carbo*-benzene 4e): A solution of hexayne **3e** (70 mg, 0.102 mmol) in Et_2O (50 mL) was treated with $SnCl_2{\cdot}2H_2O$ (387 mg, 2.04 mmol) and saturated ethereal HCl (2 M, 5 mL, 10 mmol) between −25 and −20°C for 2 h. Stirring was then continued between −20 and −10°C for 30 min. After addition of aqueous NaOH (2 M) at 0°C, the organic layer was separated and the aqueous layer extracted twice with Et_2O. The combined organic layers were washed with brine, dried with $MgSO_4$, filtered, and concentrated under reduced pressure. Several successive chromatographic runs on silica gel ($CHCl_3$) only succeeded in affording a dark-violet solid containing **4e** as a mixture with an undetermined side-product. $R_f \approx 0.51$ (heptane/EtOAc 5:5); ^{1}H NMR (500 MHz; $CDCl_3$): $\delta = 7.75$ (t, 4H; *p*-C_6H), 8.01 (t, 8H; *m*-C_6H_2), 9.58 (d, 8H; *o*-C_6H_2), 9.90 ppm (s, 2H; C*H*); Secondary signals: $\delta = 7.62$–7.70 (m, 4–5H′), 7.85–7.95 (m, 8–10H′), 8.87 (d, 2H′), 9.22–9.26 (2 d, 4H′), 9.47 ppm (s, 1H′); ^{13}C{^{1}H} NMR (125 MHz; $CDCl_3$): $\delta = 88.16$ (*C*H, C_{18} ring),

105.25 (*C*Ph), 116.32, 120.16, 123.12 (three sp*C* of the C_{18} ring), 129.53 (*p*-*C*H), 129.85 (*m*-*C*H), 130.16 (*o*-*C*H), 139.49 ppm (*ipso*-C_6H_5). The assignment is based on ^{1}H-^{13}C HSQC and HMBC spectra (Figure 8); MS (MALDI-TOF, positive mode, DMSO, matrix: dithranol): *m*/*z* (%): 526.25 (100) $[M]^+$, 527.27 (78) $[M+H]^+$; secondary peaks at *m*/*z* (%): 561.38 (25), 562.00 (39), and 563.06 (32) may correspond to a HCl adduct of **4e**.

Computational details: Geometries were fully optimized at the B3PW91/6-31G** level of theory using Gaussian98.[39] Vibrational analysis was performed at the same level in order to check that a minimum was obtained on the potential energy surface. NMR spectra were computed at the B3LYP/6-31+G** level of theory. NICS (nucleus independent chemical shift) values were computed at the same level according to the procedure described by von R. Schleyer et al.[25] The magnetic shielding tensor was calculated for a ghost atom located at the geometric center of the ring using the GIAO (gauge including atomic orbital) method implemented in Gaussian98.[40]

Acknowledgements

The authors wish to thank the Centre National de la Recherche Scientifique and the Ministère de l'Education Nationale de la Recherche et de la Technologie for Ph.D. fellowships and the ACI for financial support. The authors also gratefully acknowledge CALMIP (Calcul intensif en Midi-Pyrénées, Toulouse, France), IDRIS (Institut du Développement et des Ressources en Informatique Scientifique, Orsay, France) and CINES (Centre Informatique de l'Enseignement Supérieur, Montpellier, France) for computing facilities. The authors are also indebted to one of the referees whose critical reading and suggestions were very helpful.

[1] R. Chauvin, *Tetrahedron Lett.* **1995**, *36*, 397.
[2] a) L. T. Scott, G. J. DeCicco, J. L. Hyun, G. J. Reinhardt, *J. Am. Chem. Soc.* **1983**, *105*, 7760; b) L. T. Scott, G. J. DeCicco, J. L. Hyun, G. Reinhardt, *J. Am. Chem. Soc.* **1985**, *107*, 6546.
[3] a) C. Godard, C. Lepetit, R. Chauvin, *Chem. Commun.* **2000**, 1833; b) C. Lepetit, C. Godard, R. Chauvin, *New J. Chem.* **2001**, *25*, 572; c) C. Lepetit, B. Sivi, R. Chauvin, *J. Phys. Chem. A* **2003**, *107*, 464; d) C. Lepetit, V. Peyrou, R. Chauvin, *Phys. Chem. Chem. Phys.* **2004**, *6*, 303; e) I. Yavari, A. Jabbari, M. Samadizadeh, *J. Chem. Res. (S)* **1999**, 152.
[4] R. Chauvin, C. Lepetit, *Modern Acetylene Chemistry. Chemistry, Biology and Material Sciences* (Eds.: F. Diederich, P. J. Stang, R. R. Tykwinski), Wiley, Weinheim, **2005**, Chapter 1, p. 1.
[5] L. Maurette, C. Tedeschi, E. Sermot, M. Soleilhavoup, F. Hussain, B. Donnadieu, R. Chauvin, *Tetrahedron* **2004**, *60*, 10077.
[6] R. Chauvin, *Tetrahedron Lett.* **1995**, *36*, 401.
[7] a) Y. Kuwatani, N. Watanabe, I. Ueda, *Tetrahedron Lett.* **1995**, *36*, 119; b) R. Suzuki, H. Tsukude, N. Watanabe, Y. Kuwatani, I. Ueda, *Tetrahedron* **1998**, *54*, 2477.
[8] a) J. Rauss-Godineau, W. Chodkiewicz, P. Cadiot, *Bull. Soc. Chim. Fr.* **1966**, 2885; b) S. F. Sisenwine, A. R. Day, *J. Org. Chem.* **1967**, *32*, 1770; c) M. S. Newmen, K. Kanakarajan, *J. Org. Chem.* **1980**, *45*, 2301.
[9] C. Lepetit, C. Zou, R. Chauvin, *J. Org. Chem.* **2006**, *71*, 6317.
[10] C. Saccavini, C. Tedeschi, L. Maurette, C. Sui-Seng, M. Soleilhavoup, L. Vendier, C. Zou, R. Chauvin, *Chem. Eur. J.* **2007**, *13*, DOI: 10.1002/chem.200601191.
[11] J.-M. Ducere, C. Lepetit, P. G. Lacroix, J.-L. Heully, R. Chauvin, *Chem. Mater.* **2002**, *14*, 3332.
[12] C. Lepetit, P. G. Lacroix, V. Peyrou, C. Saccavini, R. Chauvin, *J. Comput. Methods Sci. Eng.* **2004**, *4*, 569.
[13] S. Kolotilov, R. Chauvin, unpublished results
[14] K. Nakatani, P. G. Lacroix, C. Saccavini, R. Chauvin, unpublished results.
[15] The analysis called for the ELF bifurcation tree-diagram: The critical ELF value at which all the localization domains adjacent to a given atom become irreducible (i.e., are disconnected and contain the attractor of a single valence basin of the atom) is indeed a nucleophilicity index for this atom, see: F. Fuster, A. Sevin, B. Silvi, *J. Phys. Chem. A* **2000**, *104*, 852.
[16] a) C. Lepetit, B. Sivi, R. Chauvin, *J. Phys. Chem. A* **2003**, *107*, 464; b) C. Lepetit, V. Peyrou, R. Chauvin, *Phys. Chem. Chem. Phys.* **2004**, *6*, 303.
[17] O. A. Gansow, A. R. Burke, G. N. La Mar, *J. Chem. Soc., Chem. Commun.* **1972**, 556.
[18] B. Ma, H. M. Sulzbach, Y. Xie, F. H. Schaefer III, *J. Am. Chem. Soc.* **1994**, *116*, 3529.
[19] a) Y. Rubin, C. B. Knobler, F. Diederich, *Angew. Chem.* **1991**, *103*, 708; *Angew. Chem. Int. Ed. Eng.* **1991**, *30*, 698; b) E. Abele, K. Rubina, J. Popelis, I. Mazeika, E. Lukevics, *J. Organomet. Chem.* **1999**, *586*, 184.
[20] H. B. Holmes, C. L. D. Jennings-White, A. H. Schultess, B. Akinde, D. R. M. Walton, *J. Chem. Soc., Chem. Commun.* **1979**, 840.
[21] H. Suezawa, T. Yoshida, M. Hirota, H. Takahashi, Y. Umezawa, K. Honda, S. Tsuboyama, M. Nishio, *J. Chem. Soc., Perkin Trans. 2* **2001**, 2053.
[22] R. Chauvin, *J. Phys. Chem.* **1992**, *96*, 9194.
[23] J. H. Schön, Ch. Kloc, B. Batlogg, *Science* **2001**, *293*, 2432.
[24] The *carbo*-meric **4f/4f'** redox system has been studied theoretically at the B3PW91/6-31G** level of theory and compared with the parent benzoquinone/hydroquinone system: M. Gicquel, C. Lepetit, R. Chauvin, unpublished results. For related results on carbo-oxocarbons see: C. Lepetit, H. Chermette, M. Gicquel, J.-L. Heully, R. Chauvin, *J. Phys. Chem.* **2007**, *111*, 136
[25] P. von R. Schleyer, C. Maerker, A. Dransfeld, H. Jiao, N. J. R. v. E. Hommes, *J. Am. Chem. Soc.* **1996**, *118*, 6317.
[26] A. R. Katritzky, P. Barczynski, G. Musumarra, D. Pisano, M. Szafran, *J. Am. Chem. Soc.* **1989**, *111*, 7.
[27] P. von R. Schleyer, P. K. Freeman, H. Jiao, B. Goldfuss, *Angew. Chem.* **1995**, *107*, 332; *Angew. Chem. Int. Ed. Engl.* **1995**, *34*, 337.
[28] C. Lepetit, M. B. Nielsen, F. Diederich, R. Chauvin, *Chem. Eur. J.* **2003**, *9*, 5056.
[29] The general scope of *carbo*-benzene chemistry has recently been reviewed: V. Maraval, R. Chauvin, *Chem. Rev.* **2006**, *106*, 5317.
[30] C. Zou, V. Maraval, C. Duhayon, R. Chauvin, unpublished results.
[31] C. Zou, C. Lepetit, Y. Coppel, R. Chauvin, *Pure Appl. Chem.* **2006**, *78*, 791.
[32] J. Suffert, *J. Org. Chem.* **1989**, *54*, 509.
[33] a) D. J. Watkin, C. K. Prout, J. R. Carruthers, P. W. Betteridge, CRYSTALS Issue 10, Chemical Crystallography Laboratory, Oxford, **1996**; b) SIR92 program for automatic solution of crystal structures by direct methods: A. Altomare, G. Cascarano, G. Giacovazzo, A. Guagliardi, M. C. Burla, G. Polidori, M. Camalli, *J. Appl. Crystallogr.* **1994**, *27*, 435.
[34] J. R. Carruthers, D. J. Watkin, *Acta Crystallogr. Sect. A* **1979**, *35*, 698.
[35] SHELX97 (includes SHELXS97, SHELXL97, CIFTAB), Programs for Crystal Structure Analysis (Release 97.2), G. M. Sheldrick, Institüt für Anorganische Chemie der Universität, Göttingen (Germany), **1998**.
[36] WINGX: L. J. Farrugia, *J. Appl. Crystallogr.* **1999**, *32*, 837.
[37] ORTEP3 for Windows: L. J. Farrugia, *J. Appl. Crystallogr.* **1997**, *30*, 565.
[38] *International Tables for X-Ray Crystallography, Vol. IV*, (Eds: I. A. Ibers, W. C. Hamilton), Kynoch Press, Birmingham (England), **1974**.
[39] Gaussian 98 (Revision A.7), M. J. Frisch, G. W. Trucks, H. B. Schlegel, G. E. Scuseria, M. A. Robb, J. R. Cheeseman, V. G. Zakrzewski, J. A. Montgomery, Jr., R. E. Stratmann, J. C. Burant, S. Dapprich, J. M. Millam, A. D. Daniels, K. N. Kudin, M. C. Strain, O. Farkas, J. Tomasi, V. Barone, M. Cossi, R. Cammi, B. Mennucci, C. Pomelli, C. Adamo, S. Clifford, J. Ochterski, G. A. Petersson, P. Y. Ayala, Q. Cui, K. Morokuma, D. K. Malick, A. D. Rabuck, K. Raghavachari, J. B. Foresman, J. Cioslowski, J. V. Ortiz, B. B. Stefanov, G. Liu, A. Liashenko, P. Piskorz, I. Komaromi, R. Gomperts, R. L. Martin,

D. J. Fox, T. Keith, M. A. Al-Laham, C. Y. Peng, A. Nanayakkara, C. Gonzalez, M. Challacombe, P. M. W. Gill, B. G. Johnson, W. Chen, M. W. Wong, J. L. Andres, M. Head-Gordon, E. S. Replogle, J. A. Pople, Gaussian, Inc., Pittsburgh, PA, **1998**.

[40] N. Walker, D. Stuart, *Acta Crystallogr. Sect. A* **1983**, *39*, 158.

Received: August 16, 2006
Revised: November 4, 2006
Published online: March 19, 2007

